

Decomposition aided attention-based recurrent neural networks for multistep ahead time-series forecasting of renewable power generation

Robertas Damaševičius^{Corresp.,1}, Luka Jovanovic², Aleksandar Petrovic³, Miodrag Zivkovic³, Nebojsa Bacanin³, Dejan Jovanovic⁴, Milos Antonijevic³

¹ Department of Applied Informatics, Vytautas Magnus University, Kaunas, Lithuania

² Faculty of Technical Sciences, Singidunum University, Belgrade, Serbia

³ Faculty of Informatics and Computing, Singidunum University, Belgrade, Serbia

⁴ College of academic studies "Dositej", Belgrade, Serbia

Corresponding Author: Robertas Damaševičius
Email address: robertas.damasevicius@vdu.lt

Renewable energy plays an increasingly important role in our future. As fossil fuels become more difficult to extract and effectively process, renewables offer a solution to the ever-increasing energy demands of the world. However, the shift toward renewable energy is not without challenges. While fossil fuels offer a more reliable means of energy storage that can be converted into usable energy, renewables are more dependent on external factors used for generation. Efficient storage of renewables is more difficult often relying on batteries that have a limited number of charge cycles. A robust and efficient system for forecasting power generation from renewable sources can help alleviate some of the difficulties associated with the transition toward renewable energy. Therefore, this study proposes an attention-based recurrent neural network approach for forecasting power generated from renewable sources. To help networks make more accurate forecasts, decomposition techniques utilized applied the time series, and a modified metaheuristic is introduced to optimized hyperparameter values of the utilized networks. This approach has been tested on two real-world renewable energy datasets covering both solar and wind farms. The models generated by the introduced metaheuristics were compared with those produced by other state-of-the-art optimizers in terms of standard regression metrics and statistical analysis. Finally, the best-performing model was interpreted using SHapley Additive exPlanations.

1 Decomposition aided attention-based 2 recurrent neural networks for multistep 3 ahead time-series forecasting of renewable 4 power generation

5 Robertas Damaševičius¹, Luka Jovanovic², Aleksandar Petrovic³, Miodrag
6 Zivkovic⁴, Nebojsa Bacanin⁵, Dejan Jovanovic⁶, and Milos Antonijevic⁷

7 ¹Department of Applied Informatics, Vytautas Magnus University, Kaunas, Lithuania

8 ²Faculty of Technical Sciences, Singidunum University, Belgrade Serbia

9 ^{3,4,5,7}Faculty of Informatics and Computing, Singidunum University, Belgrade Serbia

10 ⁶College of academic studies "Dositej", Belgrade, Serbia

11 Corresponding author:

12 Robertas Damaševičius¹

13 Email address: robertas.damasevicius@vdu.lt

14 ABSTRACT

15 Renewable energy plays an increasingly important role in our future. As fossil fuels become more difficult
16 to extract and effectively process, renewables offer a solution to the ever-increasing energy demands
17 of the world. However, the shift toward renewable energy is not without challenges. While fossil fuels
18 offer a more reliable means of energy storage that can be converted into usable energy, renewables
19 are more dependent on external factors used for generation. Efficient storage of renewables is more
20 difficult often relying on batteries that have a limited number of charge cycles. A robust and efficient
21 system for forecasting power generation from renewable sources can help alleviate some of the difficulties
22 associated with the transition toward renewable energy. Therefore, this study proposes an attention-based
23 recurrent neural network approach for forecasting power generated from renewable sources. To help
24 networks make more accurate forecasts, decomposition techniques utilized applied the time series, and
25 a modified metaheuristic is introduced to optimized hyperparameter values of the utilized networks. This
26 approach has been tested on two real-world renewable energy datasets covering both solar and wind
27 farms. The models generated by the introduced metaheuristics were compared with those produced by
28 other state-of-the-art optimizers in terms of standard regression metrics and statistical analysis. Finally,
29 the best-performing model was interpreted using SHapley Additive exPlanations.

30 1 INTRODUCTION

31 The role of renewable energy is a paramount factor in sustainability of the society. Traditional energy
32 systems usually based on fossil fuels are not efficient and require more complicated processes of extraction.
33 The demands of human civilization are always growing, which exposes the difficulties for eco-friendly
34 energetic growth. As renewable energy source (RES) become more available the distribution of new
35 resources in the network result in stochasticity, intermittency, and uncertainty. Consequentially, the
36 traditional energy systems are dominant in the share of energy used amounting to 81% of the global
37 share Loe (2022).

38 For RES to become more widely utilized, the previously mentioned challenges need to be overcome.
39 Additionally, energy storage on a smaller scale remains difficult when working with RES, in comparison
40 to fossil fuel storage, which is still considered more reliable. The storage of electricity is mostly achieved
41 by batteries which are a limited resource on their own due to the limited number of life cycles for each
42 one of them Zhang and Zhao (2023). All things considered, a possible solution is a mechanism that can
43 provide accurate forecasts of the amount of resources being generated from RES. Such a solution would
44 have to be able to analyze short-term time series and provide a robust mechanism as it affects electricity

45 load and its price. Electricity traders and system operators are most affected by these changes.

46 Traditional methods for regression have previously been applied to forecasting RES power produc-
47 tion Foley et al. (2012); Abuella and Chowdhury (2015) However, as the world's need for energy increases
48 further improvements are needed in order to make forecasting methods viable. A major challenge when
49 tackling RES production forecasting comes from the noisy nature of the data. Since renewable resources
50 rely on natural phenomena such as wind or solar exposure, many chaotic factors play a role in the amount
51 of power that can be produced. Nevertheless, patterns in this data are still present, though often difficult
52 to initially observe.

53 By applying advanced signal processing techniques, such as decomposition techniques, strong signals
54 can be separated from the noise, allowing prediction methods to focus on determining correlations between
55 signals with strong patterns rather than those heavily affected by noise. This concept has often been
56 applied to systems that require precise moments in noise environments such as electroencephalogra-
57 phy Murariu et al. (2023) demonstrating great potential. Several decomposition techniques have been
58 developed in recent years such as empirical mode decomposition (EMD) Boudraa and Cexus (2007)
59 and ensemble empirical mode decomposition (EEMD) Wu and Huang (2009). While efficient, the lack
60 of a strong mathematical background in these methods has led to the development of variational mode
61 decomposition (VMD) Dragomiretskiy and Zosso (2013) that has shown great potential for tackling signal
62 decomposition with a strong mathematical basis.

63 One additional approach that has shown great potential when working with data catheterized by
64 complex nonlinear relations is the application of artificial intelligence (AI). Powerful AI algorithms are
65 capable of improving their performance through an iterative data-driven process. By observing data
66 AI algorithms can determine correlations without explicit programming. This makes AI a promising
67 approach for tackling this pressing issue. Nevertheless, the performance of modern algorithms is reliant on
68 proper hyperparameter selection. With increasing numbers of hyperparameters, traditional methods such
69 as trial and error have become insufficient to optimize algorithm performance. The use of metaheuristic
70 optimization algorithms provides a potential solution for efficient hyperparameter selection.

71 Forecasting power generation can be formulated as a time series forecasting challenge. By doing so,
72 algorithms capable of responding to data sequences can be leveraged in order to make more accurate
73 forecasts. One promising approach, that extensive literature review suggests has not yet sufficiently been
74 explored when applied to renewable forecasting, is the use of recurrent neural networks (RNN) Medsker
75 and Jain (1999). These networks represent a variety of artificial neural networks (ANN) that allow
76 previous inputs to affect future outputs, making them highly suitable for time series forecasting. A
77 recent improvement incorporates attention mechanisms Olah and Carter (2016) into RNN allowing
78 networks to focus their attention on specific features improving accuracy. Additionally, the literature
79 review suggests that attention-based RNNs (RNN-ATT) have not yet been applied to renewable power
80 forecasting, indicating a gap in research that this work hopes to address. Exploring the potential of these
81 networks is essential as a robust forecasting method could help make RES more viable and lower the
82 world's dependence on fossil fuels.

83 This research proposes an approach that applies a neural network model based on attention for that
84 purpose. Moreover, the proposed model was applied to two different problems including the Spain
85 wind and solar energy predictions and the wind farms in China predictions. Datasets for both countries'
86 surveys have been used with the RNN model and the attention-based recurrent neural network RNN-ATT.
87 However, these networks require fine-tuning of a large number of hyperparameters, that can result in non-
88 deterministic polynomial time complexity (NP-hard). Hyperparameter optimization is done through the
89 use of metaheuristics, and a modified version of the well-known harris hawk optimization (HHO) Heidari
90 et al. (2019) algorithm is introduced. Two sets of experiments have been carried out both with RNN and
91 RNN-ATT networks, applied to each real-world dataset.

92 This research is an extension of previous researches in this domain Bacanin et al. (2023b); Stoean et al.
93 (2023); Bacanin et al. (2023a), where the long short-term (LSTM), bidirectional LSTM (BiLSTM) and
94 gated recurrent unit (GRU) were applied for RES forecasting challenges. However, the goal of this work
95 is to test lighter models (classical RNNs) for problems of RES with the application of fewer neurons over
96 layers while providing satisfactory performance. Additionally, conversely to previous experimentation's,
97 current research also investigates the potential of RNNs with attention mechanism and it was validated
98 against different RES time-series datasets. Also, the classical RNNs (without attention mechanism) were
99 also validated in order to establish the influence of attention layer to overall network performance.

100 The primary contributions of this work can be summarized as the following:

- 101 • The RNN-ATT-based method for forecasting RES power generation.
- 102 • A modified version of a metaheuristic tasked with selecting network parameters.
- 103 • The application of the introduced approach to two real-world datasets to determine their potential
104 for real-world use.
- 105 • The interpretation of the best generated RNN models that can be used as a valuable tools for renew-
106 able energy specialists to determine which factor has the most influence on the RES performance.

107 The structure of the paper includes Section 2 for providing the technological fundamentals for the
108 performed experiments. Section 3 explains the original version of the applied metaheuristic as well as
109 the modified version. Section 4 explains the utilized datasets in detail and gives information on the test
110 setup. The outcomes are presented in Section 5, followed by a discussion. statistical validation and model
111 interpretation presented in Section 6. Finally, Section 7 concluded the work and presents potential future
112 research.

113 2 BACKGROUND AND PRELIMINARIES

114 This section introduces techniques required for reader to have a full and insightful understanding of
115 experiments conducted in this research.

116 2.1 Time-Series Decomposition and Integration

117 Time-series decomposition is a technique used to break down a time-series data into its constituent
118 components, such as trend, seasonality, and residual (noise). By decomposing a time-series, we can better
119 understand the underlying patterns and relationships within the data, which can, in turn, improve the
120 accuracy and reliability of time-series forecasting models like the Luong attention-based RNN model.

121 2.1.1 Decomposition Techniques

122 Various decomposition techniques can be applied to time-series data, including:

123 **1. Classical Decomposition:** This method decomposes a time-series into its trend, seasonal, and
124 residual components using moving averages and seasonal adjustments. There are two primary approaches
125 in classical decomposition: additive and multiplicative. In the additive decomposition, the time-series
126 is expressed as the sum of its components, while in the multiplicative decomposition, the time-series is
127 expressed as the product of its components.

128 **2. Seasonal and Trend decomposition using Loess (STL):** STL is a flexible and robust decomposi-
129 tion method that uses locally weighted regression (Loess) to estimate the trend and seasonal components
130 of a time-series. It can handle both constant and time-varying seasonality, as well as arbitrary patterns of
131 missing data. The STL method also allows for user-defined control over the smoothness and periodicity
132 of the seasonal and trend components.

133 **3. Seasonal Decomposition of Time Series (SDTS):** SDTS is an extension of the classical decompo-
134 sition method that incorporates a seasonal adjustment factor for each observation in the time-series. This
135 factor is obtained by dividing the observed value by the corresponding seasonal component. The seasonal
136 adjustment factors can be used to deseasonalize the time-series, which can then be analyzed for trend and
137 residual components.

138 **4. Wavelet Transform:** Wavelet transform is a mathematical technique used to decompose a time-
139 series into a set of wavelet coefficients, which represent the time-series at different scales and resolutions.
140 Wavelet transform can capture both the low-frequency (trend) and high-frequency (seasonal and noise)
141 components of a time-series, making it a powerful tool for time-series decomposition and analysis.

142 **5. Empirical Mode Decomposition:** Empirical Mode Decomposition (EMD) is a powerful and
143 flexible technique for analyzing non-stationary and non-linear time series data. Introduced by Huang
144 et al. Huang et al. (1998), EMD is designed to adaptively decompose a time series into a finite set of
145 intrinsic mode functions (IMFs) that capture the local oscillatory behavior of the signal at various scales.
146 The primary goal of EMD is to provide a data-driven decomposition that does not rely on any predefined
147 basis functions or assumptions about the underlying signal characteristics Abayomi-Alli et al. (2020). By
148 incorporating EMD into the renewable power generation forecasting process, we can potentially enhance

149 the accuracy, reliability, and interpretability of the forecasting models, ultimately aiding in the efficient
150 management and planning of renewable energy resources.

151 **2.1.2 Variational mode decomposition**

152 The VMD Dragomiretskiy and Zosso (2013) technique used for signal decomposition builds upon the
153 solid foundation established but other methods. However, VMD does so with a strong mathematical
154 foundation compared to empirical techniques. Signal modes of varying frequencies are extracted from the
155 original signal original signals by finding modes that are orthogonal to each other with localized frequency
156 content. The decomposition is achieved through progressive optimization according to Eq. (1).

$$E(V) = \int \left(\frac{1}{2} \|V'(t)\|_2^2 + \mu U(V(t)) \right) dt \quad (1)$$

157 in which $V(t)$ are signal modes, $V'(t)$ denotes the derivative of $V(t)$ with respect to time. Additionally
158 the regularization parameter μ balances between extracted mode smoothness and sparsity. Accordingly,
159 function $U(V(t))$ promotes sparsity.

160 The decomposition process is handled by an algorithm that switches between solving modes and
161 determines the penalty. Minimizing the energy function modes can be determined with respect to $V(t)$. A
162 Lagrange multiplier $\alpha(t)$ is also introduced giving Eq. (2).

$$E(V) = \int \left(\frac{1}{2} \|V'(t)\|_2^2 + \mu U(V(t)) + \alpha(t) \sum_{k=1}^K V_k(t)^2 \right) dt \quad (2)$$

163 where the k -th mode of a signal is represented by $V_k(t)$. In order to revise the penalty function, the energy
164 function is minimized with respect to $\alpha(t)$. To accomplish this, the derivative of $E(V)$ with respect to
165 $\alpha(t)$ is set to zero. The resulting function is shown in Eq. (3)

$$\frac{d}{dt} \alpha(t) = \mu \sum_{k=1}^K V_k(t)^2 - \lambda \quad (3)$$

166 with the λ constraint defining the overall mode energy.

167 **2.1.3 Integration of Decomposed Components**

168 Once the time-series has been decomposed into its constituent components, the next step is to integrate
169 these components into the forecasting model. There are several ways to incorporate the decomposed
170 components into the Luong attention-based RNN model:

171 **1. Component-wise Modeling:** Train separate RNN models for each of the decomposed components
172 (trend, seasonal, and residual), and then combine the forecasts from these models to obtain the final forecast
173 for the original time-series. This approach can help in capturing the unique patterns and dependencies
174 within each component more effectively.

175 **2. Feature Augmentation:** Use the decomposed components as additional input features to the
176 RNN model, along with the original time-series. This approach can help the model in learning the
177 relationships between the decomposed components and the target variable, potentially improving the
178 model's forecasting performance.

179 **3. Preprocessing:** Deseasonalize the time-series by removing the seasonal component before training
180 the RNN model, and then add back the seasonal component to the model's forecasts to obtain the final
181 forecast for the original time-series. This approach can help in reducing the complexity of the time-series
182 and make it easier for the model to capture the underlying trend and residual patterns.

183 **4. Postprocessing:** Train the RNN model on the original time-series, and then adjust the model's
184 forecasts using the decomposed components (e.g., by adding the seasonal component to the model's
185 forecasts). This approach can help in correcting the model's forecasts for any systematic errors or biases
186 related to the seasonal component.

187 2.2 Recurrent neural network

188 Time series prediction is the motivation for the improvements in artificial neural networks (ANN) Pascanu
189 et al. (2013). The difference from the multilayer perceptron is that the hidden unit links are enabled with a
190 delay. The results of such modifications allow the model to be sensitive toward temporal data occurrences
191 of greater length.

192 RNNs are considered as a high-performing solution but further improvements were applied to achieve
193 even greater performance. The main issues are the exploding and vanishing gradient. The solution was
194 provided with long short-term memory (LSTM) model. The reason for not using the latest solution is that
195 sometimes RNNs tend to outperform LSTMs as they introduce a large number of hyperparameters that
196 can sometimes hinder performance Bas et al. (2021).

197 The advantage of the RNN as well is that it does not have to take inputs of fixed vector length, in
198 which case the output has to be fixed as well. While working with rich structures and sequences this
199 advantage can be exploited. In other words, the model works with input vectors and is able to generate
200 sequences on the output. The RNN processes the data of the sequence while the hidden state is held.

201 2.3 Luong attention-based model

202 The attention phenomenon is not defined by mathematics and its application in the Luong attention-based
203 model should be considered as a mechanism. Some examples of different mathematical expression
204 applications of the attention mechanism are the sliding window methods, saliency detection, local image
205 features, etc. Regarding the attention mechanism application in the case of an RNN, the definition is
206 precise.

207 The networks that can work with the attention mechanism and possess RNN characteristics are
208 considered attention-based. The purpose of such a mechanism is to work with different weights for the
209 sequence in input. The data can be captured as a result and input-output relations are usable. The basic
210 solution of such architecture is the application of a second RNN.

211 The authors chose the Luong attention-based model for that purpose. Weight represented as w_t is
212 calculated for the source for every timestep t for the decoding of attention-based encoder-decoder as
213 $\sum_s w_t(s) = 1$ and $\forall s w_t(s) \geq 0$. The hidden state h_t has a function that is the related timestep's predicted
214 token, while the $\sum_s w_t(s) * \hat{h}_s$.

215 Different mathematical applications of the attention mechanism differ in the way they compute
216 weights. In the case of the Luong model, it is the softmax function on the scaled scores of each token.
217 Matrix W_a linearly transforms the decoder's h_t dot product and the encoder \hat{h}_s to calculate the score.

218 2.4 Hyperparameters of Luong-attention based RNN

219 The Luong attention-based RNN model is an extension of the basic RNN model with the addition of an
220 attention mechanism that allows the model to selectively focus on different parts of the input sequence
221 when generating the output. The following hyperparameters are typically involved in the configuration of
222 the Luong attention-based RNN model:

223 **1. Number of hidden layers (n_{hid}):** The number of hidden layers in the RNN architecture, which
224 determines the depth of the model. A larger number of hidden layers can enable the model to capture
225 more complex patterns and dependencies in the data but may also increase the risk of overfitting and
226 require more computational resources.

227 **2. Number of hidden units per layer (n_{unit}):** The number of hidden units (neurons) in each hidden
228 layer of the RNN. A larger number of hidden units can increase the model's capacity to learn complex
229 patterns, but it may also increase the risk of overfitting and require more computational resources.

230 **3. Type of RNN cell:** The choice of RNN cell used in the model, such as Long Short-Term
231 Memory (LSTM) or Gated Recurrent Unit (GRU). These cells are designed to better handle long-range
232 dependencies and mitigate the vanishing gradient problem compared to the traditional RNN cells.

233 **4. Attention mechanism:** The specific attention mechanism used in the model. In the case of the
234 Luong attention-based RNN model, the attention mechanism can be of two types: global or local attention.
235 Global attention attends to all the source positions, while local attention focuses only on a small window
236 of source positions around the current target position.

237 **5. Attention scoring function:** The scoring function computes the alignment scores between the
238 source and target sequences in the attention mechanism. Luong et al. proposed three different scoring
239 functions: dot product, general (multiplicative), and concatenation (additive). The choice of scoring
240 function can affect the model's performance and interpretability.

241 **6. Learning rate (α):** The learning rate is a critical hyperparameter that controls the size of the
242 updates to the model's weights during the training process. A smaller learning rate might lead to more
243 precise convergence but require more training iterations, while a larger learning rate may speed up the
244 training process but risk overshooting the optimal solution.

245 **7. Dropout rate (p_{drop}):** The dropout rate is a regularization technique used to prevent overfitting in
246 neural networks. During training, a fraction of the neurons in the network is randomly "dropped out" or
247 deactivated, with the specified dropout rate determining the proportion of neurons deactivated at each
248 training iteration.

249 **8. Batch size:** The number of training samples used in a single update of the model's weights. A
250 larger batch size can lead to more accurate gradient estimates and faster training but may require more
251 memory and computational resources.

252 **9. Sequence length:** The length of input and output sequences used in the model. Longer se-
253 quences may allow the model to capture more extensive temporal dependencies but can also increase the
254 computational complexity and risk of overfitting.

255 These hyperparameters play a crucial role in determining the performance of the Luong attention-
256 based RNN model for renewable power generation forecasting. Selecting optimal values for these
257 hyperparameters requires careful experimentation, and metaheuristic optimization techniques like the
258 Harris Hawk Optimization algorithm can be helpful in this process.

259 **2.5 Metaheuristic Optimization**

260 In recent years model optimization has become a popular topic in computer science. Increasing model
261 complexity, as well as growing numbers of hyperparameters of modern algorithms, has made it necessary
262 to develop techniques to automate this process, which was traditionally handled through trial and error.
263 However, this is a challenging task, as selecting optimal parameters is often a mixed NP-hard problem,
264 with both discreet and continuous values having a role to play in defining model performance. A powerful
265 group of algorithms capable of addressing NP-hard problems within reasonable time constraints and
266 with realistic computational demands are metaheuristic optimization algorithms. By formulating the
267 process of parameter selection as an optimization task, metaheuristics can be employed to efficiently
268 improve performance. A notably popular group of metaheuristics is swarm intelligence that models
269 observed behaviors of cooperating groups to perform optimizations. Some notable algorithms that have
270 become popular for tackling optimization tasks among researchers include the Harris hawk optimizer
271 (HHO) Heidari et al. (2019), genetic algorithm GA Mirjalili and Mirjalili (2019), particle swarm optimizer
272 (PSO) Kennedy and Eberhart (1995), artificial bee colony (ABC) Karaboga (2010) algorithm, firefly
273 algorithm (FA) Yang and Slowik (2020). Additionally the LSHADE for Constrained Optimization
274 with Levy Flights (COLSHADE) algorithm Gurrola-Ramos et al. (2020) and Self-Adapting Spherical
275 Search (SASS) Zhao et al. (2022) are notable recent examples of optimizers. These algorithms, and
276 algorithms derived from their base have been applied in several fields with promising outcomes. Some
277 noteworthy examples of metaheuristics applied to optimization problems include examples for crude oil
278 price forecasting Jovanovic et al. (2022) and industry 4.0 Jovanovic et al. (2023).

279 **3 PROPOSED METHOD**

280 This section begins with a brief overview of the basic HHO algorithm, followed by explanation and
281 justifications of the modifications that were made to the original method.

282 **3.1 Original Harris hawk optimization**

283 The inspiration for the HHO are the attack strategies of the bird with the same name. The phases of
284 attacks can be differentiated as exploration, the transition to exploitation, and the exploitation. The
285 algorithm was introduced by Heidari et al. Heidari et al. (2019) and has been used for a wide variety of
286 optimization-related applications such as machine scheduling Jouhari et al. (2020) and neural network
287 optimization Ali et al. (2022).

In the first phase, the exploration, the goal is the global optimum. Multiple locations in the population
serve for random initialization which mimics the hawk's search for prey. The parameter q controls this

process as it switches between two strategies of equal probability:

$$X(t+1) = \begin{cases} X_{rand}(t) - r_1|X_{rand}(t) - 2r_2X(t)|, q \geq 0 \\ (X_{best}(t) - X_m(t)) - r_3(LB + r_4(UB - LB)), q < 0.5, \end{cases} \quad (4)$$

in which the random number from the range $[0, 1]$ are r_1 , r_2 , r_3 , and r_4 as well as q and these numbers are updated on an iteration basis. The position vector of the solution in the next iteration is $X(t+1)$, and the positions of the solutions of the best, current, and average solutions in the current iteration t are given respectively as $X_{best}(t)$, $X(t)$ and $X_m(t)$, while the lower bound is LB and the upper bound is UB . The average position is provided by a simple averaging approach:

$$X_m(t) = \frac{1}{N} \sum_{i=1}^N X_i(t), \quad (5)$$

288 for which N shows the total solutions number, and the individual X at iteration t is shown as $X_i(t)$.

The term prey energy is introduced as it indicates if the algorithm should revert back to exploration and so forth. The solutions updates strength in each iteration as:

$$E = 2E_0(1 - \frac{t}{T}), \quad (6)$$

289 for T as iteration maximum for a run, the prey's initial energy E_0 which varies inside the $[-1, 1]$ interval.

290 The exploitation phase represents the literal attack of the hawk and maps out its behavior as it is
291 closing in. The mathematical translation is given as $|E| \geq 0.5$ for more passive attacking, and $|E| < 0.5$
292 otherwise.

In cases where the prey of the hawk is still at large, the hawks encircle the prey with the goal of exhaustion which is modeled as follows:

$$X(t+1) = \Delta X(t) - E|JX_{best}(t) - X(t)| \quad (7)$$

$$\Delta X(t) = X_{best}(t) - X(t), \quad (8)$$

where the vector difference of the best solution (prey) and the current solution in iteration t is shown as $\Delta X(t)$. The strategy of the prey's escape is controlled by the random attribute J which differs from iteration to iteration:

$$J = 2(1 - r_5), \quad (9)$$

for which the interval $[0, 1]$ maps out the random value r_5 . For $r \geq 0.5$ and $|E| < 0.5$ the prey is considered exhausted and more aggressive attack strategies are applied. For this case, the current position is updated as :

$$X(t+1) = X_{best}(t) - E|\Delta X(t)| \quad (10)$$

If the prey is still not giving up the hawks apply another attack strategy called zig-zag movements commonly known as leapfrog movements. Following equation evaluates if such behavior should be applied:

$$Y = X_{best}(t) - E|JX_{best}(t) - X(t)|, \quad (11)$$

while the leapfrog movements are modeled as:

$$Z = Y + S \times LF(D), \quad (12)$$

in which the problem dimension is given as D , a random vector of $1 \times D$ size as S , and the levy flight LF calculated by:

$$LF(x) = 0.01 \times \frac{u \times \sigma}{|v|^{\frac{1}{\beta}}}, \sigma = \left(\frac{\Gamma(1 + \beta) \times \sin(\frac{\pi\beta}{2})}{\Gamma(\frac{1+\beta}{2}) \times \beta \times 2^{(\frac{\beta-1}{2})}} \right)^{\frac{1}{\beta}} \quad (13)$$

Consequently, the position updating mechanism is provided:

$$X(t+1) = \begin{cases} Y, & \text{if } F(Y) < F(X(t)) \\ Z, & \text{if } F(Z) < F(X(t)), \end{cases} \quad (14)$$

293 where the eqs. (11) and (12) are utilized for calculating the Y and Z .

Lastly, for the case of $r \leq 0.5$ and $|E| < 0.5$ the prey is considered to be out of energy, and stronger attacks are applied with rapid drive progressively. The distance between the target before its acquisition is modeled as:

$$X(t+1) = \begin{cases} Y, & \text{if } F(Y) < F(X(t)) \\ Z, & \text{if } F(Z) < F(X(t)), \end{cases} \quad (15)$$

for which the Y and Z are obtained by the next two equations:

$$Y = X_{best}(t) - E|JX_{best}(t) - X(t)| \quad (16)$$

$$Z = Y + S \times LF(D) \quad (17)$$

294 **3.2 Proposed enhanced Harris Hawk optimization algorithm**

295 **3.2.1 New initialization scheme**

296 The applied approach exploits a novel initialization strategy of populations:

$$x_{i,j} = lb_j + \psi \cdot (ub_j - lb_j), \quad (18)$$

297 in which the j -th component of i -th solution is given as $x_{i,j}$, the upper and lower bounds are standardly
298 ub_j and lb_j for the parameter j , and a pseudo-random number is drawn between $[0, 1]$ and given as ψ .

299 The quasi-reflection-based learning (QRL) procedure has proven to give results Jovanovic et al. (2023)
300 where applied with the goal of sarge space enlargement for the case of those generated by the (18).
301 Hence the x_j^{qr} , quasi-reflexive-opposite component for all parameters of a solution x_j is provided as in the
302 following equation:

$$X_j^{qr} = \text{rnd} \left(\left[\frac{lb_j + ub_j}{2}, x_j \right], x_j \right), \quad (19)$$

303 while at $\left[\frac{lb_j + ub_j}{2}, x_j \right]$ interval a pseudo-random number is chosen as rnd .

Algorithm 1 QRL pseudo-code initialization scheme

- 1: P^{init} population with $N/2$ solutions created by Eq. (18).
 - 2: P^{qr} population by QRL from P^{init} by Eq. 19.
 - 3: Merge P^{init} and P^{qr} ($P \cup P^{qr}$) resulting in the starting population.
 - 4: Fitness calculation of every solution in P
 - 5: P sorted by fitness
-

304 **3.2.2 Mechanism for maintaining population diversity**

305 Diversification is observed as a parameter of the convergence/divergence ratio during the search process
306 as in Cheng and Shi (2011).

307 $L1$ norm Cheng and Shi (2011) applies two-component diversification for the solutions and the
308 dimensions of the problem. Important information for the search process can be derived from the
309 dimension-wise metric with the $L1$ norm.

310 The number of total individuals is marked with m and the dimensions number as n , the $L1$ norm is
311 given as in Eqs. 20 -22:

$$\bar{x} = \frac{1}{m} \sum_{i=1}^m x_{ij} \quad (20)$$

$$D_j^p = \frac{1}{N} \sum_{i=1}^N |x_{ij} - \bar{x}_j| \quad (21)$$

$$D^p = \frac{1}{n} \sum_{i=1}^n D_j^p \quad (22)$$

312 in which every individual's position mean is represented as \bar{x} vector over all dimensions, the hawk's
 313 position vector of diversity as $L1$ norm is shown as D_j^p , while the scalar form is shown as D^p for the
 314 entire population. Using regular strategies of initialization usually results in higher diversity with weaker
 315 convergence towards later iterations. The described metric is used for $L1$ determination of the threshold
 316 D_t for the diversity. Firstly, the D_{t0} is calculated by Eq. 23, which is followed by condition $D^p < D_t$
 317 for the satisfactory value of diversity, the worst solutions are replaced with randomly generated solutions nrs
 318 with the same strategy for population initialization. The nrs value is another control parameter.

$$D_{t0} = \sum_{j=1}^n \frac{(ub_j - lb_j)}{2 \cdot n} \quad (23)$$

319 The Eq. (1) and Algorithm 1 indicate close generation of solutions towards the bounds of the search
 320 space's mean. The value D_t falls off as shown in:

$$D_{t,iter+1} = D_{t,iter} - D_{t,iter} \cdot \frac{iter}{T}, \quad (24)$$

321 in which the current and subsequent iterations are given as $iter$ and $iter + 1$, and the number of iterations
 322 at the maximum is T . According to this mechanism, the D_t falls off in no relation to the D^p and still will
 323 not trigger the mechanism.

324 **3.2.3 Inner workings and complexity of proposed method**

325 Taking inspiration from applied mechanisms to the original solution the proposed new algorithm is
 326 diversity directed HHO (DDHHO). It is important to note that the computational complexity of the
 327 original algorithm is not lower than that of the novel solution. In modern literature, it is a practice
 328 to measure this in FFEs as it is the most resource-demanding technique, hence the complexity of the
 329 DDHHO for the worst scenario is Yang and He (2013): $O(DDHHO) = O(N) + O(T \cdot N^2)$

330 **3.3 Hyperparameter optimization using HHO**

331 To optimize the hyperparameters of the Luong attention-based RNN model, we perform the following
 332 steps:

333 **Define the search space:** Identify the hyperparameters to be optimized and specify their respective
 334 ranges or discrete sets of possible values. For instance, for the number of hidden layers, we may specify a
 335 range of values, e.g., from 1 to 5. Similarly, we define the search space for other hyperparameters such as
 336 the number of hidden units per layer, type of RNN cell, attention mechanism, attention scoring function,
 337 learning rate, dropout rate, batch size, and sequence length.

338 **Initialize the population:** Generate an initial population of candidate solutions, where each candidate
 339 solution represents a combination of hyperparameter values within the defined search space.

340 **Evaluate candidate solutions:** For each candidate solution, train the Luong attention-based RNN
 341 model using the specified hyperparameter values, and evaluate the model's performance on a validation
 342 set using one or more performance metrics (e.g., MAE, RMSE, and MAPE). This step may require
 343 cross-validation or other validation techniques to obtain reliable performance estimates.

Algorithm 2 Pseudo-code of the basic HHO algorithm implementation

Inputs: The population size N and maximum number of iterations T
Outputs: The location of the rabbit and its fitness value
Initialize the random population $X_i (i = 1, 2, \dots, N)$
Initialize population $X_i, (i = 1, 2, 3, \dots, N)$ according to Algorithm 1
Determine values of D_{t0} and D_t
while (stopping condition is not met) **do**
 Calculate the fitness values of hawks
 Set X_{rabbit} as the location of rabbit (best location)
 for (each hawk (X_i)) **do**
 Update the initial energy E_0 and jump strength J
 Update the E using Eq. (6)
 if ($|E| \geq 1$) **then**
 Update the location vector using Eq. (4)
 end if
 if ($|E| < 1$) **then**
 if ($r \geq 0.5$ and $|E| \geq 0.5$) **then**
 Update the location vector using Eq. (7)
 else if ($r \geq 0.5$ and $|E| < 0.5$) **then**
 Update the location vector using Eq. (10)
 else if ($r < 0.5$ and $|E| \geq 0.5$) **then**
 Update the location vector using Eq. (14)
 else if ($r < 0.5$ and $|E| < 0.5$) **then**
 Update the location vector using Eq. (15)
 end if
 end if
 Calculate D^p
 if ($D^p < D_t$) **then**
 Replace worst nrs with solutions created as in (18)
 end if
 Update D_t by expression (24)
 end while
Return X_{rabbit}

344 **Apply optimization algorithm:** Utilize the chosen metaheuristic optimization algorithm to explore
345 the search space and find the best combination of hyperparameter values that minimizes the chosen
346 performance metric(s). In each iteration, the algorithm updates the candidate solutions based on the
347 optimization strategy specific to the chosen algorithm, and the performance of the updated solutions is
348 re-evaluated on the validation set.

349 **Termination condition:** The optimization process continues until a predefined termination condition
350 is met, such as a maximum number of iterations, a minimum performance improvement threshold, or a
351 predefined computational budget.

352 **Select the optimal solution:** Once the termination condition is reached, select the candidate solution
353 with the best performance on the validation set as the optimal combination of hyperparameter values for
354 the Luong attention-based RNN model.

355 **Final model training and evaluation:** Train the Luong attention-based RNN model using the optimal
356 hyperparameter values on the entire training set, and evaluate its performance on the test set to obtain an
357 unbiased estimate of the model's forecasting accuracy.

358 4 DATASET DESCRIPTION AND EXPERIMENTS

359 This section aims to provide an overview of the datasets utilized in the experiments and the experimental
360 setup established for all methods employed in the comparative analysis.

361 4.1 Utilized Datasets

362 4.1.1 Spain Solar Energy Dataset

363 The first dataset, concerning photovoltaic power generation in Spain, is constructed from real-world
364 originating from two different sources. The ENTSO-E portal ¹ provides hourly energy demand and
365 generation considering the renewable energy in Spain, while the weather data is provided by OpenWeather
366 API ² for the location of Valencia, Spain.

367 Considering the large amount of data available, a smaller dataset segment was utilized during exper-
368 imentation. The datasets cover hourly data from 1.8.2018. to 31.12.2018. and covered a total of 3670
369 data points. Most relevant hourly metrics are included for multivariate forecasting as well as the data and
370 support metrics of generated photovoltaic power. The dataset was then further separated and with 70% of
371 the data used for training, 10% for validation, and the remaining 20% for testing. The included features
372 include generated photovoltaic power, as well as humidity, rainfall, cloud cover, and ambient temperature.
373 With the generated photovoltaic power feature being the prediction target.

374 4.1.2 China Wind Farm Dataset

375 The Global Energy Forecasting Competition 2012 (GEFCom2012) is a competition that aimed to promote
376 the development of state-of-the-art forecasting models for various aspects of the energy industry. The
377 dataset related to wind farms in China used in a competition ³. Seven wind farms from mainland China
378 were selected and anonymized for this dataset. Power generation data has been normalized as well due to
379 anonymity concerns.

380 Relevant wind data is collected every 12h while the dataset includes forecasts in intervals of 24h.
381 The direction and speed of the wind and meridional wind components are provided as well. The dataset
382 consists of hourly measurements of wind power generation from seven wind farms located in China,
383 spanning from January 1, 2011, to September 30, 2012. Each wind farm has different installed capacities,
384 which makes the forecasting task more challenging. For experimentation, hourly resolution data has
385 been split into predictions of 12h and then further combined with normalized real-world data of power
386 generation for each farm by the hour. Due to the last year of data not being available, the dataset consists
387 of four years of data. The included features are Wind speed, wind direction, and zonal and meridional
388 wind components for each wind farm while the target feature is the amount of generated power.

389 The first 70% of the available data points were utilized for training, while the later 10% and 20% were
390 used for validation and testing.

391 4.1.3 Data Preprocessing

392 Before using the dataset for renewable power generation forecasting, some preprocessing steps may be
393 necessary:

- 394 1. **Missing Data Imputation:** The dataset may contain missing values, which need to be imputed
395 before using the data for model training and evaluation. Various imputation techniques can be
396 employed, such as linear interpolation or more advanced methods based on machine learning
397 models.
- 398 2. **Data Splitting:** Divide the dataset into training, validation, and testing subsets. The training and
399 validation sets can be used for model development and hyperparameter tuning, while the testing set
400 can be used for the final evaluation of the forecasting model's performance.
- 401 3. **Feature Engineering:** Extract additional features from the dataset that may be relevant for the
402 forecasting task, such as lagged values of wind power, moving averages, or other temporal features
403 that can help capture the patterns and dependencies in the data.
- 404 4. **Normalization/Standardization:** Scale the input features and target variable to ensure that they
405 are on a similar scale, which can improve the performance and stability of the forecasting model.

406 Once the dataset is preprocessed, it can be used to train and evaluate various forecasting models, such
407 as the Luong attention-based RNN model discussed earlier. By incorporating techniques like time-series

¹<https://transparency.entsoe.eu/>

²<https://openweathermap.org/guide>

³<https://www.kaggle.com/competitions/global-energy-forecasting-competition-2012-load-forecasting/data>

408 decomposition, attention mechanisms, and hyperparameter optimization, the forecasting models can
409 be tailored to the specific characteristics and challenges of the wind power generation data, ultimately
410 improving the accuracy and reliability of the forecasts.

411 4.2 Experimental Setup

412 The following setup regards all 4 test cases that have been executed. Two stages are differentiated
413 during experimentation. During the first, the data is decomposed for both test cases. Afterward, the
414 signal components and residual signals are provided to the RNN for forecasting. Every tested model
415 was provided in the same manner with historic data of six input points per model for three steps ahead
416 predictions.

417 The data was split in the same manner for all four test cases, with the training set amounting to 70%,
418 the validation set of 10%, and the testing set of 20%. The split of each the solar dataset target features is
419 visualized with Figure 1 to illustrate the time intervals that were employed in each of the three mentioned
420 subsets. Similarly, the wind dataset is shown in Figure 2.

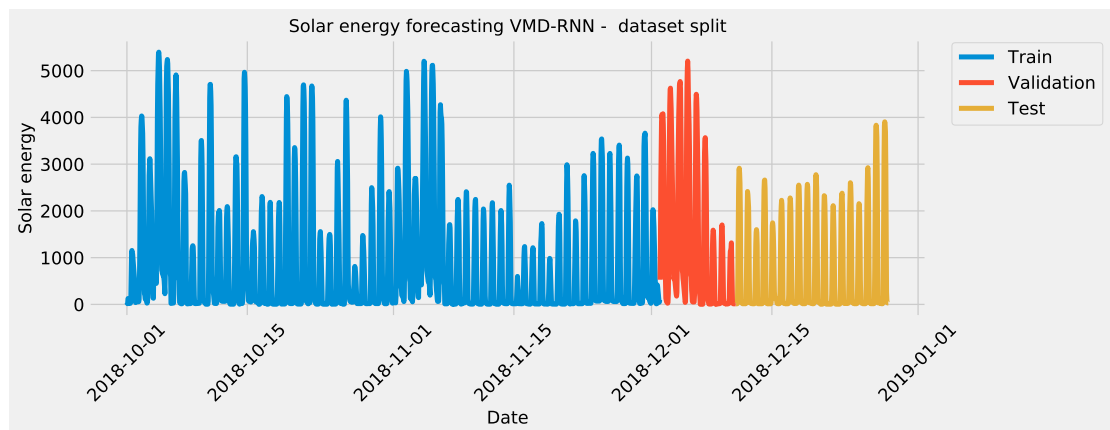


Figure 1. Solar energy generation target feature split

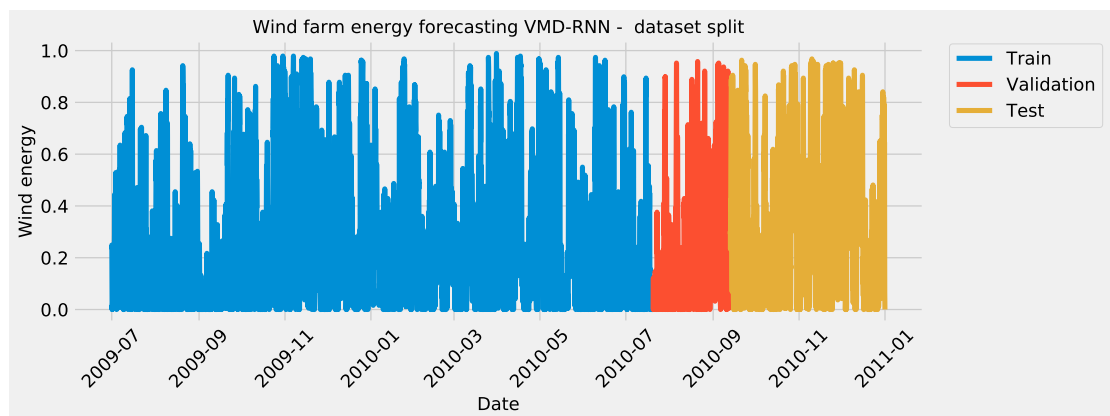


Figure 2. Wind energy generation target feature Split

421 The challenge of parameter optimization for the prediction models was tested on the following
422 contemporary metaheuristics: genetic algorithm (GA) Mirjalili and Mirjalili (2019), particle swarm
423 optimization (PSO) Kennedy and Eberhart (1995), artificial bee colony (ABC) Karaboga (2010), firefly
424 algorithm (FA) Yang and Slowik (2020), COLSHADE Gurrola-Ramos et al. (2020), and self-adaptive
425 step size algorithm Tang and Gibali (2020). Additionally, to the mentioned metaheuristics the original
426 HHO and the DDHHO were evaluated.

427 The parameters for the VMD were empirically established and the parameter $K = 3$, while the α
428 parameter represents the length of the used dataframe. To ensure the objectivity of model evaluation

429 30 independent runs were performed due to the stochastic nature of the optimization algorithms. The
 430 selected parameters for optimization of the RNN are given in the following text due to their impact on the
 431 performance of the model. The ranges of the parameters alongside their descriptions are given: [50, 100]
 432 number of neurons, [0.0001, 0.01] learning rate, [100, 300] training epochs, [0.05, 0.1] dropout rate, and
 433 [1, 3] for the total layer number of a network.

434 Lastly, an early stopping mechanism is incorporated for overfitting prevention with the threshold
 435 empirically determined as $\frac{epochs}{3}$. The purpose of such a mechanism is to terminate the model early if
 436 no improvements are observed for $\frac{epochs}{3}$. It should be noted that this approach reduces computational
 437 resource waste.

438 In this study, we employ five commonly used performance metrics to evaluate the accuracy and
 439 effectiveness of the proposed attention-based recurrent neural network (A-RNN) model for renewable
 440 power generation forecasting. These performance metrics are mean absolute error (MAE), root mean
 441 squared error (RMSE), mean absolute error (MAE), Coefficient of determination (R^2) and the index of
 442 alignment (IA).

443 MAE is the average of the absolute differences between the predicted values and the actual values. It
 444 measures the magnitude of errors in the forecasts without considering their direction. The MAE is defined
 445 as:

$$MAE = \frac{1}{N} \sum_{i=1}^N |y_i - \hat{y}_i| \quad (25)$$

446 where N is the number of data points, y_i is the actual value, and \hat{y}_i is the predicted value.

447 RMSE is the square root of the average of the squared differences between the predicted values and
 448 the actual values. It provides a measure of the overall model's performance by penalizing larger errors
 449 more than smaller errors. The RMSE is defined as:

$$RMSE = \sqrt{\frac{1}{N} \sum_{i=1}^N (y_i - \hat{y}_i)^2} \quad (26)$$

450 where N is the number of data points, y_i is the actual value, and \hat{y}_i is the predicted value.

451 MAE is the average of the absolute differences between the predicted values and the actual values.
 452 It can be useful for comparing the performance of different models across various scales. The MAE is
 453 defined as:

$$MAE = \frac{1}{n} \sum_{i=1}^n |y_i - \hat{y}_i| \quad (27)$$

454 where N is the number of data points, y_i is the actual value, and \hat{y}_i is the predicted value and $||$ denotes
 455 absolute values.

456 R^2 indicates the proportion of the variance in the dependent variable that can be explained by the
 457 independent variables in the model. It ranges from 0 to 1, with higher values indicating a better fit between
 458 the model and the data. R^2 is defined as:

$$R^2 = 1 - \frac{\sum_i (y_i - \hat{y}_i)^2}{\sum_i (y_i - \bar{y})^2} \quad (28)$$

459 where N is the number of data points, y_i is the actual value, \hat{y}_i is the predicted value and \bar{y} refers to the
 460 mean of the actual values.

461 IA measures the extent to which the model's predicted outcomes align with the true outcomes or the
 462 intended goals. A higher Alignment Index indicates a stronger alignment, suggesting that the model is
 463 performing well. AI is defined as:

$$IA = 1 - \frac{\sum_{i=1}^n (y_i - \hat{y}_i)^2}{\sum_{i=1}^n (|y_p - \bar{y}| + |y_i - \bar{y}|)^2} \quad (29)$$

464 where N is the number of data points, y_i is the actual value, \hat{y}_i is the predicted value, \bar{y} refers to the mean
 465 of the actual values and $||$ denotes absolute values.

466 These performance metrics, MAE, RMSE, and MAPE, are used to evaluate the accuracy and effec-
 467 tiveness of the proposed A-RNN model in comparison to the regular RNN model for renewable power
 468 generation forecasting. A lower value for each metric indicates better forecasting performance.

469 A flowchart of the utilized experimental framework is provided in Figure 3.

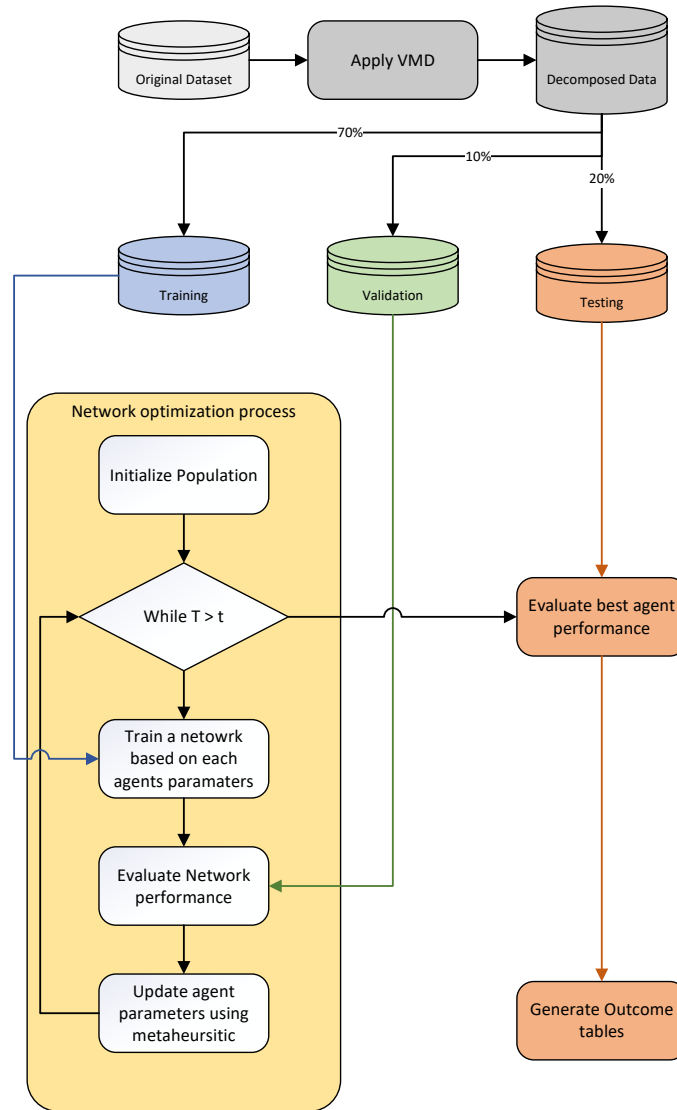


Figure 3. Experimental framework flowchart

470 5 RESULTS AND COMPARISON

471 This section exhibits obtained experimental findings in terms of captured performance metrics. The best
 472 metrics in all tables were marked with bold style to more clearly visualize the best performing methods.

473 5.1 Spain Solar Energy Forecasting

474 In Table 1 the objective function outcomes for the best, worst, mean, and median executions, alongside
 475 the standard deviance with variance are shown for 30 independent runs of each metaheuristic.

Table 1. VMD-RNN solar energy forecasting objective function overall outcomes

Method	Best	Worst	Mean	Median	Std	Var
VMD-RNN-DDHHO	0.006284	0.007320	0.006855	0.006931	0.000389	1.513667E-7
VMD-RNN-HHO	0.006990	0.007890	0.007366	0.007282	0.000344	1.183526E-7
VMD-RNN-GA	0.006664	0.007559	0.007061	0.007228	0.000341	1.163809E-7
VMD-RNN-PSO	0.007186	0.007458	0.007345	0.007425	0.000115	1.320113E-8
VMD-RNN-ABC	0.006499	0.007231	0.006830	0.006801	0.000251	6.319240E-8
VMD-RNN-FA	0.007005	0.007542	0.007184	0.007014	0.000229	5.253891E-8
VMD-RNN-COLSHADE	0.007159	0.008009	0.007478	0.007182	0.000357	1.273813E-7
VMD-RNN-SASS	0.007057	0.007405	0.007264	0.007240	0.000135	1.829039E-8

476 As Table 1 suggests, the introduces algorithms attained the best results when optimizing a RNN in the
 477 best run. However, admirable stability was demonstrated by the PSO. Furthermore, when considering the
 478 worst case execution the ABC attained the best results as well as in the mean and median runs. This is to
 479 be expected as per the NFL Wolpert and Macready (1997) no single approach works equally well in all
 480 execution cases.

481 Further detailed metrics for the best run, for each forecasting step and every tested metaheuristic are
 482 demonstrated in Table 2.

Table 2. The VMD-RNN solar energy metrics per each step

Step	Metric	VMD-RNN-DDHHO	VMD-RNN-HHO	VMD-RNN-GA	VMD-RNN-PSO	VMD-RNN-ABC	VMD-RNN-FA	VMD-RNN-COLSHADE	VMD-RNN-SASS
One Step	R ²	0.601739	0.549365	0.627364	0.528460	0.58500	0.544636	0.543719	0.559259
	MAE	384.294171	432.200603	396.006180	427.516283	404.377133	418.018708	411.089031	412.655917
	MSE	400081.633100	452694.787317	374338.747453	473694.873874	416895.063424	457445.578253	458366.263037	442755.336455
	RMSE	632.520065	672.825971	611.832287	688.254948	645.674115	676.347232	677.027520	665.398630
	IA	0.886044	0.870430	0.896802	0.870911	0.877714	0.875709	0.875988	0.877386
Two Step	R ²	0.8896686	0.878472	0.844966	0.868775	0.876350	0.885817	0.873014	0.8760918
	MAE	195.801662	227.673953	246.869567	233.834781	227.774440	204.845965	216.919114	219.607867
	MSE	110835.615218	122082.984352	155742.443523	131825.249471	124214.713878	114704.662015	127566.656326	124474.546886
	RMSE	332.919833	349.403755	394.642172	363.077470	352.441079	338.680767	357.164747	352.809505
	IA	0.970558	0.966796	0.960179	0.966048	0.965562	0.969940	0.968305	0.966947
Three Step	R ²	0.962557	0.964848	0.948636	0.978350	0.973942	0.960881	0.961240	0.951496
	MAE	122.562368	137.209296	165.046855	105.082911	112.980142	141.060131	124.093137	141.036372
	MSE	37613.696545	35313.037867	51598.255163	21749.216531	26177.198226	39297.213129	38936.684159	48725.218704
	RMSE	193.942508	187.917636	227.152493	147.4761560	161.793690	198.235247	197.323805	220.737896
	IA	0.9901459	0.990594	0.986690	0.994450	0.992991	0.989871	0.990657	0.987153
Overall	R ²	0.817988	0.797562	0.806989	0.791861	0.811765	0.797111	0.792658	0.795616
	MAE	234.219400	265.694617	269.307534	255.477992	248.377238	254.641602	250.700427	257.766719
	MSE	182843.648288	203363.603179	193893.148713	209089.779959	189095.658509	203815.817799	208289.867841	205318.367348
	RMSE	427.602208	450.958538	440.332998	457.263360	434.851306	451.459652	456.387848	453.120698
	IA	0.948916	0.942607	0.947890	0.943803	0.945423	0.945173	0.944983	0.943829

483 As can be observed in Table 2 the introduces method attained the best overall results in all cases
 484 except the R² metric, where the PSO attained better results. As the guiding objective function during the
 485 optimization process was MSE this is to be expected. Additionally the introduces method also attained
 486 the best results when making forecasts two steps ahead, as well MAE for one step ahead. The best results
 487 for R², MSE and IA where attained by the GA, while the best RMSE results where attained by the PSO.
 488 Nevertheless when making forecasts three steps ahead the PSO attained the best results across all metrics
 489 except R² where the FA attained the best outcomes.

490 To help demonstrated the improvements made by the introduced method visualizations are provided
 491 for the distribution of both MSE and R² are shown in Figure 4 followed by convergence plots for both
 492 functions in Figure 5 and swarm and KDE plots in Table 6.

493 Finally, the parameters selected by each metaheuristic for their respective best models are shown in
 494 Table 3.

495 Similarly to the previous experiment, in Table 4 the objective function outcomes for the best, worst,
 496 mean, and median executions, alongside the standard deviance with variance are shown for 30 independent
 497 runs of each metaheuristic.

498 Interestingly, when optimizing the RNN-ATT models, the introduced metaheuristic demonstrated
 499 better performance overall most metrics. However, the ABC and SASS algorithms demonstrated a slightly
 500 higher degree of stability despite attaining less impressive results.

501 Further detailed metrics for the best run, for each forecasting step and every tested metaheuristic are
 502 demonstrated in Table 5.

503 As can be observed in Table 5 the introduces method attained the best overall results for MSE and

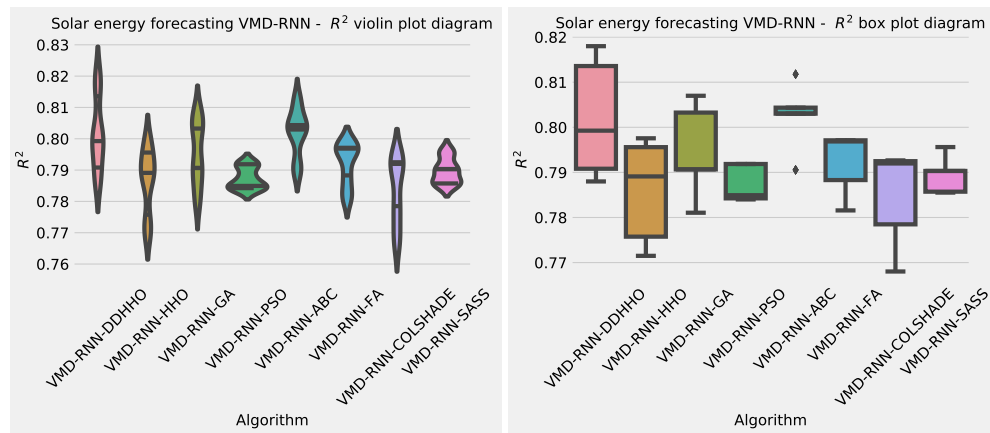


Figure 4. Solar dataset objective function and R^2 distribution plots for each metaheuristic without attention layer

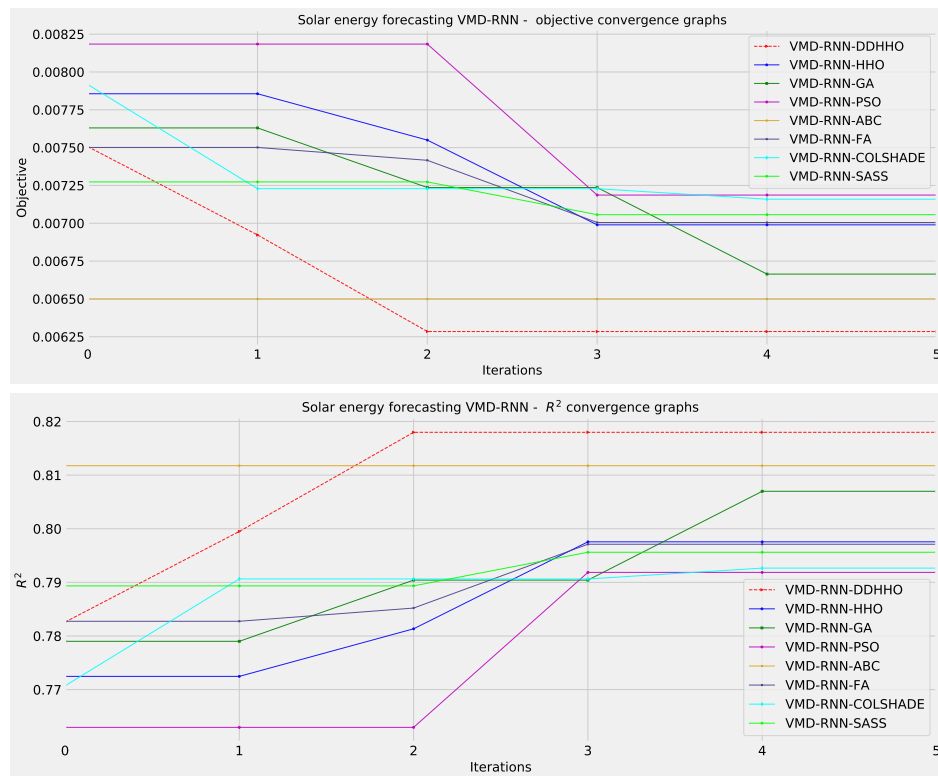


Figure 5. Solar dataset objective function and R^2 convergence plots for each metaheuristic without attention layer

504 MAE, while the HHO attained the best IA results, the ABC attained the best R^2 outcomes overall, while
 505 SASS attained the best outcomes for MAE. The introduced approach demonstrated the best performance
 506 when making predictions one step ahead, while two step ahead forecasts are done best by the PSO. No
 507 single approach performed the best for three steps ahead, while different metaheuristics attaining first
 508 place in different metrics further enforcing the NFL Wolpert and Macready (1997) theorem.

509 Visualizations of objective function and R^2 distributions are shown in Figure 7 followed by their
 510 respective convergence graphs in Figure 8. The KDE and swarm plots are also provided in Figure 9.

511 The parameters selected by each competing metaheuristic for their respective best-performing models
 512 are shown in Table 6.

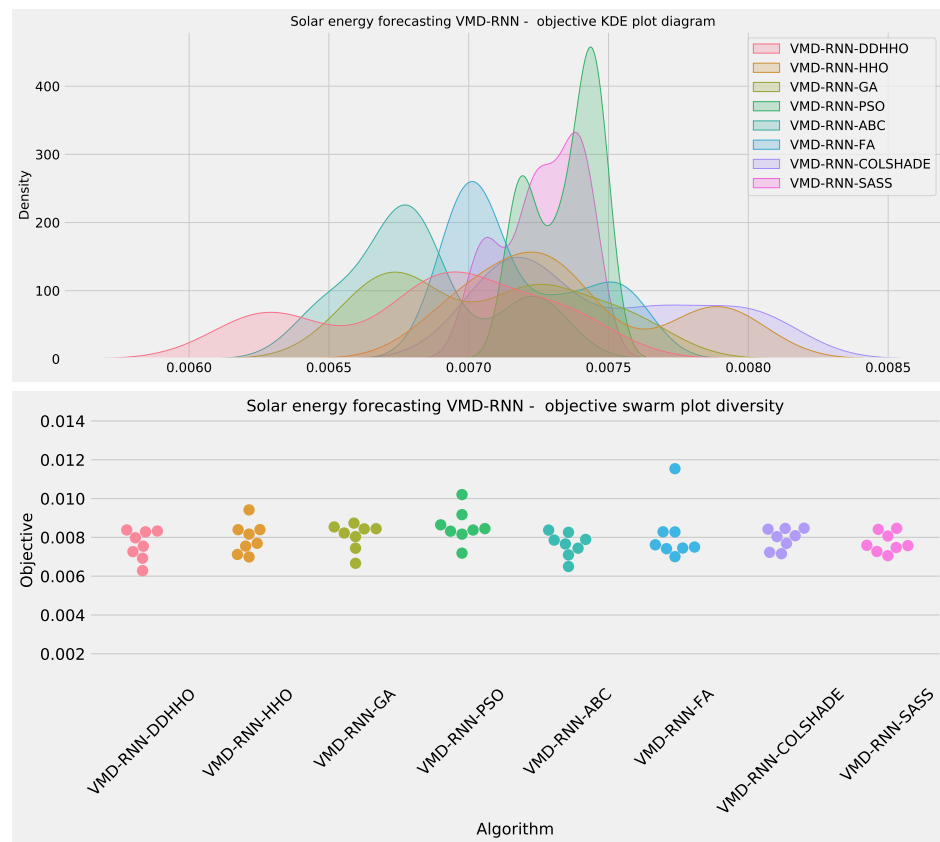


Figure 6. Solar dataset objective swarm and KDE plots for each metaheuristic without attention layer

Table 3. Parameters for best performing solar prediction RNN model optimized by each metaheuristic

Method	Learning Rate	Drouput	Epochs	Layers	L1 Neurons	L2 Neurons	L3 Neurons
VMD-RNN-DDHHO	0.007050	0.050000	232	3	50	100	100
VMD-RNN-HHO	0.007349	0.076853	206	3	64	50	100
VMD-RNN-GA	0.009097	0.091104	114	2	89	52	/
VMD-RNN-PSO	0.009329	0.069591	223	2	69	89	/
VMD-RNN-ABC	0.010000	0.100000	181	3	92	64	79
VMD-RNN-FA	0.010000	0.088052	238	2	50	50	/
VMD-RNN-COLSHADE	0.008718	0.063527	288	3	85	100	100
VMD-RNN-SASS	0.006645	0.096538	300	3	100	86	54

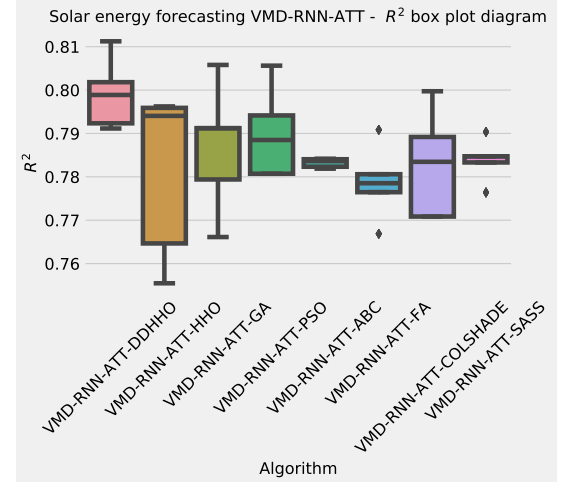
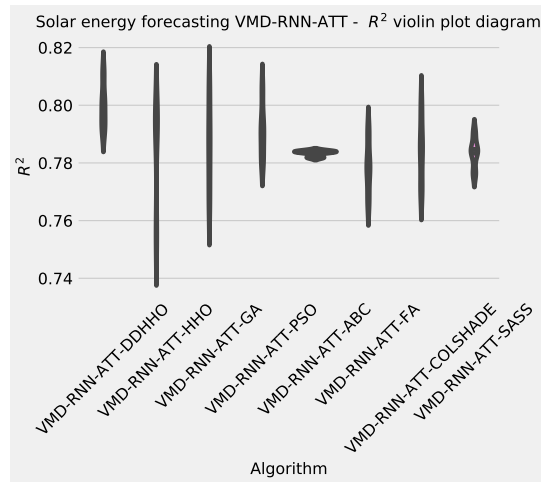
Table 4. VMD-RNN-ATT solar energy forecasting objective function overall outcomes

Method	Best	Worst	Mean	Median	Std	Var
VMD-RNN-ATT-DDHHO	0.006517	0.007211	0.006923	0.006944	0.000250	6.265266E-8
VMD-RNN-ATT-HHO	0.007036	0.008443	0.007447	0.007111	0.000613	3.759833E-7
VMD-RNN-ATT-GA	0.006705	0.008075	0.007389	0.007209	0.000499	2.490886E-7
VMD-RNN-ATT-PSO	0.006711	0.007571	0.007233	0.007303	0.000297	8.818285E-8
VMD-RNN-ATT-ABC	0.007452	0.007531	0.007480	0.007470	0.000032	1.025433E-9
VMD-RNN-ATT-FA	0.007222	0.008049	0.007641	0.007647	0.000292	8.550797E-8
VMD-RNN-ATT-COLSHADE	0.006915	0.007912	0.007455	0.007476	0.000363	1.318140E-7
VMD-RNN-ATT-SASS	0.007238	0.007720	0.007472	0.007432	0.000164	2.673677E-8

513 In Table 7 the objective function outcomes for the best, worst, mean, and median executions, alongside
 514 the standard deviance with variance are shown for 30 independent runs of each metaheuristic forecasting
 515 wind power generation.

Table 5. The VMD-RNN-ATT solar energy metrics per each step

Step	Metric	VMD-RNN-ATT-DDHHO	VMD-RNN-ATT-HHO	VMD-RNN-ATT-GA	VMD-RNN-ATT-PSO	VMD-RNN-ATT-ABC	VMD-RNN-ATT-FA	VMD-RNN-ATT-COLSHADE	VMD-RNN-ATT-SASS
1	R ²	0.715471	0.584499	0.598188	0.574065	0.603103	0.548291	0.616813	0.547094
	MAE	376.979586	442.064510	462.047919	435.538303	474.267738	435.524720	423.718303	416.220384
	MSE	285829.818133	417399.667275	403648.569532	427881.634339	398711.291244	453773.352978	384938.817726	454976.265366
	RMSE	534.630544	646.064755	635.333432	654.126620	631.435896	673.627013	620.434378	674.519285
	IA	0.9146240	0.889628	0.881474	0.871310	0.891814	0.873488	0.887386	0.861529
2	R ²	0.829019	0.876223	0.874955	0.888033	0.837797	0.868852	0.874406	0.861896
	MAE	252.954113	243.425326	260.158326	218.732420	290.688281	236.760030	252.883363	233.639125
	MSE	171162.088320	124342.580437	125616.779871	112478.817327	162944.638909	131747.397307	126168.484562	138735.683810
	RMSE	414.441900	352.622433	354.424576	335.378618	403.6640174	362.970243	355.202033	372.472393
	IA	0.951127	0.967796	0.965910	0.967226	0.958823	0.966348	0.966094	0.961092
3	R ²	0.889236	0.927962	0.9442501	0.954781	0.911610	0.955364	0.907969	0.962090
	MAE	244.240630	219.831502	179.063882	144.828299	232.407156	154.496558	244.166959	131.982225
	MSE	111269.990578	72366.697870	56004.659587	45425.756743	88793.700643	44840.040944	92451.964057	38082.907643
	RMSE	333.571567	269.010590	236.653036	213.133190	297.982719	211.754672	304.059146	195.14842
	IA	0.968308	0.980827	0.985080	0.987410	0.976862	0.988566	0.974996	0.989529
Overall	R ²	0.811242	0.796228	0.805798	0.805626	0.784170	0.790836	0.799729	0.790360
	MAE	291.391443	301.77378	300.423376	266.366341	332.454391	275.593769	306.922875	260.613911
	MSE	189620.632344	204702.981861	195090.002997	195262.069470	216816.543599	210120.263743	201186.422115	210598.285607
	RMSE	435.454512	452.441136	441.689940	441.884679	465.635634	458.388769	448.538094	458.909888
	IA	0.944686	0.946083	0.944154	0.941982	0.942500	0.942801	0.942826	0.937383

**Figure 7.** Solar dataset objective function and R^2 distribution plots for each metaheuristic with attention layer**Table 6.** Parameters for best performing solar prediction RNN-ATT model optimized by each metaheuristic

Method	Learning Rate	Drouput	Epochs	Layers	L1 Neurons	L2 Neurons	L3 Neurons	ATT Neurons
VMD-RNN-ATT-DDHHO	0.010000	0.100000	100	3	100	100	50	50
VMD-RNN-ATT-HHO	0.009323	0.100000	100	1	98	/	/	50
VMD-RNN-ATT-GA	0.009990	0.080219	148	2	71	69	/	82
VMD-RNN-ATT-PSO	0.008559	0.097184	166	3	89	51	99	96
VMD-RNN-ATT-ABC	0.010000	0.067651	101	1	50	/	/	50
VMD-RNN-ATT-FA	0.006927	0.052260	216	2	90	87	/	97
VMD-RNN-ATT-COLSHADE	0.004221	0.050000	120	1	50	/	/	71
VMD-RNN-ATT-SASS	0.009982	0.099805	188	3	100	50	50	50

516 5.2 China Wind Farm Forecasting

Table 7. VMD-RNN wind energy forecasting objective function overall outcomes

Method	Best	Worst	Mean	Median	Std	Var
VMD-RNN-DDHHO	0.010465	0.011162	0.010747	0.010764	0.000244	5.930160E-8
VMD-RNN-HHO	0.011407	0.011707	0.011538	0.011517	0.000125	1.559006E-8
VMD-RNN-GA	0.011028	0.011461	0.011240	0.011256	0.000168	2.812603E-8
VMD-RNN-PSO	0.011000	0.011507	0.011258	0.011294	0.000186	3.459674E-8
VMD-RNN-ABC	0.010729	0.010977	0.010847	0.010834	0.000108	1.176703E-8
VMD-RNN-FA	0.010519	0.011483	0.011102	0.011134	0.000381	1.448697E-7
VMD-RNN-COLSHADE	0.010823	0.011382	0.011214	0.011341	0.000241	5.784354E-8
VMD-RNN-SASS	0.011042	0.011300	0.011231	0.011298	0.000100	9.963395E-9

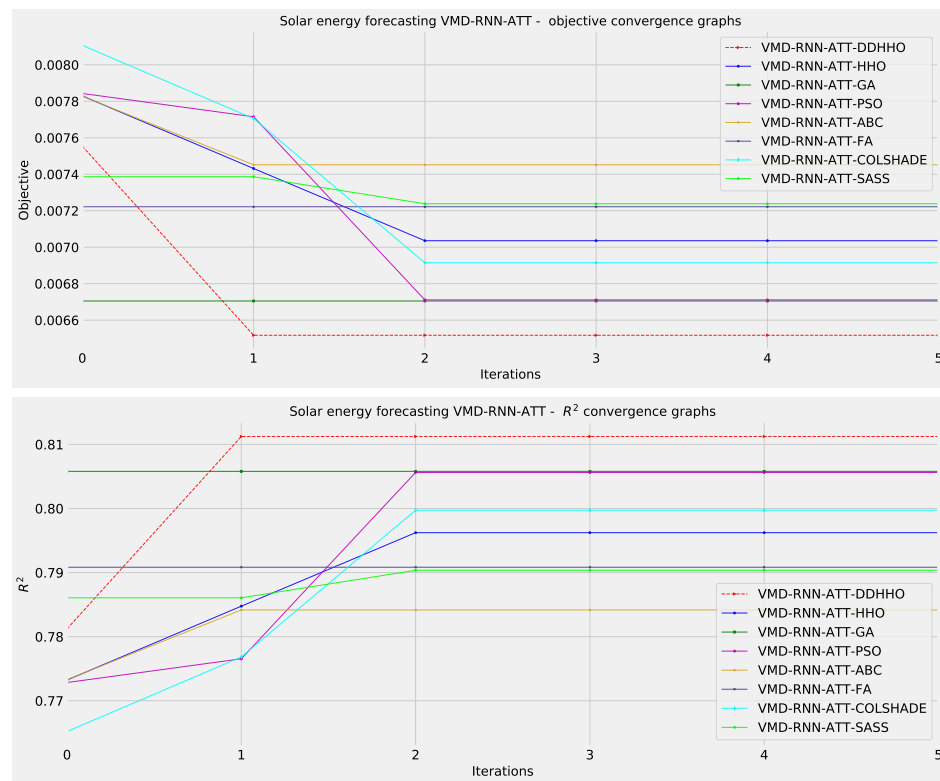


Figure 8. Solar dataset objective function and R^2 convergence plots for each metaheuristic with attention layer

517 The introduced metaheuristic attained the best outcomes in the best, mean and median executions,
 518 with the ABC attained the best outcomes in the worst case executions. Furthermore, the highest stability
 519 was demonstrated by SASS. Further detailed metrics for the best run, for each forecasting step and every
 520 tested metaheuristic are demonstrated in Table 8.

Table 8. The VMD-RNN wind energy metrics per each step

Step	Metric	VMD-RNN-DDHHO	VMD-RNN-HHO	VMD-RNN-GA	VMD-RNN-PSO	VMD-RNN-ABC	VMD-RNN-FA	VMD-RNN-COLSHADE	VMD-RNN-SASS
One Step	R^2	0.875214	0.855404	0.856190	0.849434	0.861770	0.872224	0.857508	0.861647
	MAE	0.077761	0.084168	0.083139	0.084909	0.081714	0.078881	0.083685	0.081844
	MSE	0.012012	0.013919	0.013843	0.014494	0.013306	0.012300	0.013716	0.013318
	RMSE	0.109599	0.117979	0.117658	0.120390	0.115352	0.110905	0.117117	0.115404
	IA	0.967674	0.960717	0.961990	0.958739	0.962434	0.966699	0.962278	0.962725
Two Step	R^2	0.897775	0.892783	0.900496	0.903051	0.900259	0.902827	0.899419	0.899132
	MAE	0.070751	0.074085	0.070576	0.070070	0.070933	0.070237	0.071078	0.071742
	MSE	0.009840	0.010321	0.009578	0.009332	0.009601	0.009354	0.009682	0.009710
	RMSE	0.099198	0.101592	0.097869	0.096605	0.097986	0.096716	0.098397	0.098538
	IA	0.973272	0.971041	0.973894	0.974067	0.973158	0.974287	0.973057	0.973069
Three Step	R^2	0.908009	0.904098	0.907150	0.9121979	0.910908	0.904295	0.913157	0.902638
	MAE	0.067910	0.071199	0.069404	0.0681129	0.068257	0.070842	0.066382	0.072017
	MSE	0.008855	0.009232	0.008938	0.0084520	0.008576	0.009213	0.008360	0.009372
	RMSE	0.094102	0.096081	0.094540	0.0919348	0.092607	0.095982	0.091431	0.096810
	IA	0.975517	0.974068	0.975414	0.9765410	0.976470	0.974705	0.976785	0.973296
Overall	R^2	0.893666	0.884095	0.887945	0.8882271	0.890979	0.893116	0.890028	0.887805
	MAE	0.072141	0.076484	0.074373	0.0743641	0.073635	0.073320	0.073715	0.075201
	MSE	0.010236	0.011157	0.010787	0.0107594	0.010494	0.010289	0.010586	0.010800
	RMSE	0.101172	0.105627	0.103858	0.1037274	0.102443	0.101434	0.102888	0.103923
	IA	0.972154	0.968608	0.970433	0.9697823	0.970688	0.971897	0.970706	0.969697

521 As demonstrated in Table 8, the introduced metaheuristic outperformed all competing metaheuristic
 522 in overall outcomes. The introduced metaheuristic demonstrated the best results for one step ahead
 523 forecasts; However, the PSO attained the best results for two steps ahead forecasts, and COLSHADE
 524 attained the best outcomes for three steps ahead. These results further reinforce that no single approach
 525 is equally suited to all use-cases as per the NFL Wolpert and Macready (1997) Visualizations of the
 526 distribution and convergence rates of the mse and R^2 functions are shown in Figure 10 and Figures 11.
 527 Additionally, KDE and swarm diversity plots are provided in Figure 12.

528 The network hyperparameters selected by each metaheuristic for the respective best performing

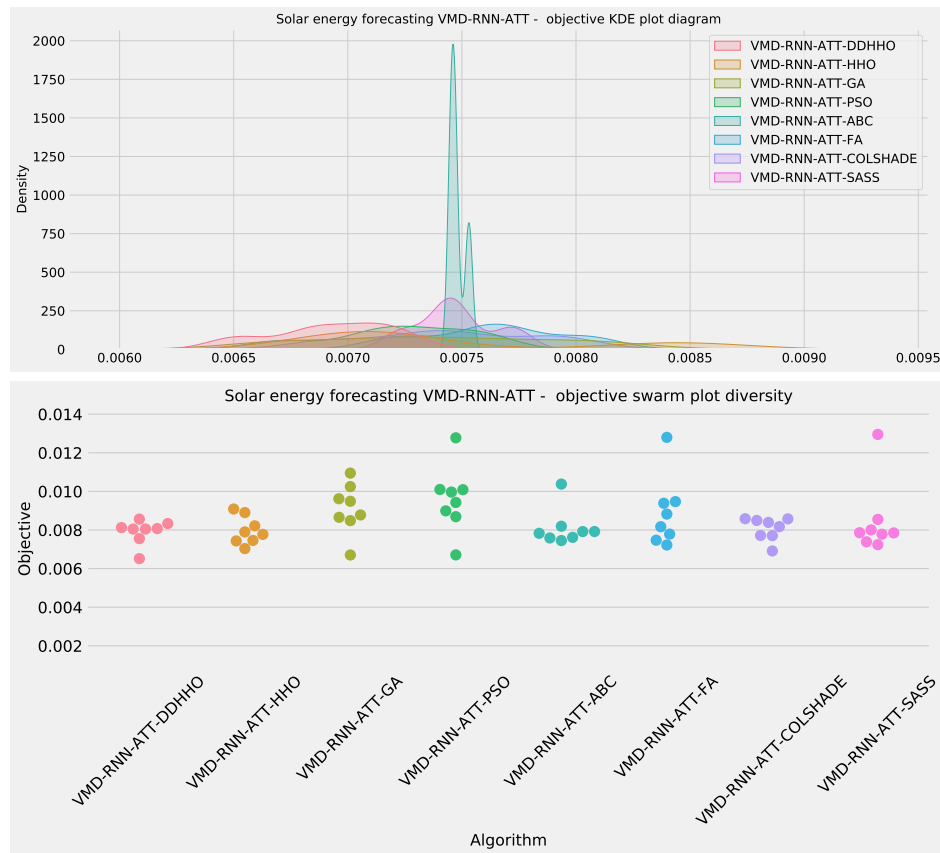


Figure 9. Solar dataset objective swarm and KDE plots for each metaheuristic with attention layer

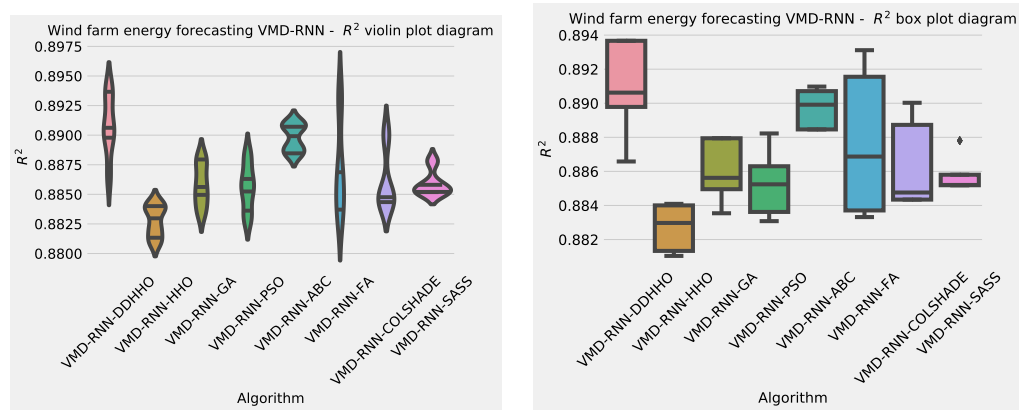


Figure 10. Wind dataset objective function and R^2 distribution plots for each metaheuristic without attention layer

529 models are shown in Table 9.

530 Similarly to the previous experiment, in Table 10 the objective function outcomes for the best, worst,
 531 mean, and median executions, alongside the standard deviance with variance are shown for 30 independent
 532 runs of each metaheuristic.

533 As it can be observed in Table 10 the introduced metaheuristic attained the best outcomes in all except
 534 the medial case, where the ABC algorithms attained the best results. Further detailed metrics for the best
 535 run, for each forecasting step and every tested metaheuristic are demonstrated in Table 11.

536 As Table 11 demonstrates, the introduces algorithms performed admirably, attaining the best outcomes

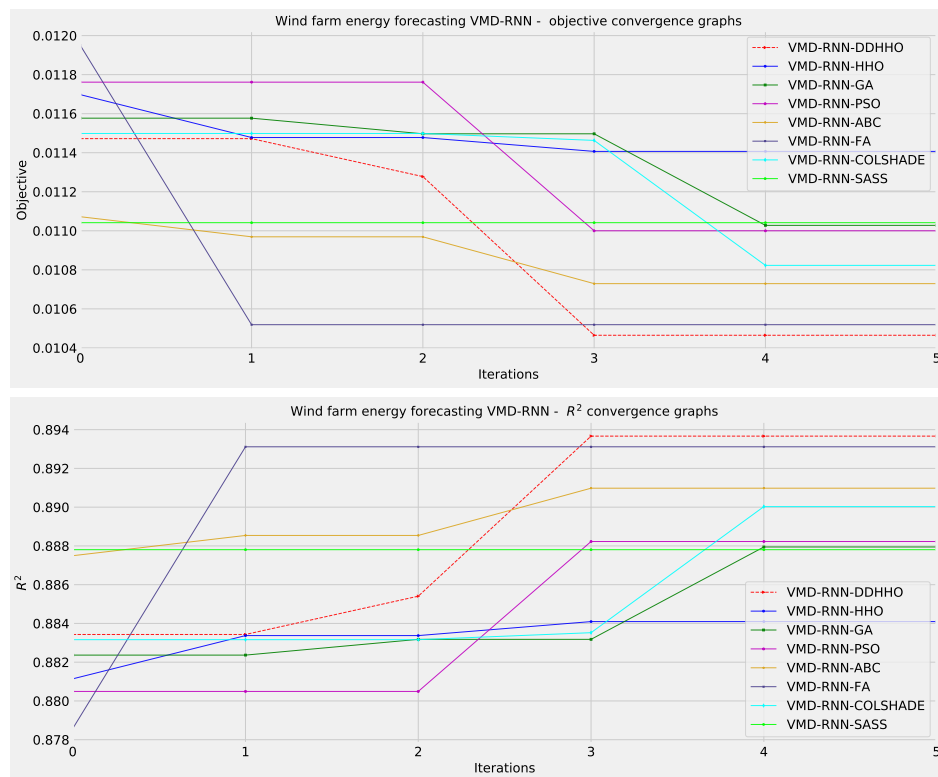


Figure 11. Wind dataset objective function and R^2 convergence plots for each metaheuristic without attention layer

Table 9. Parameters for best performing wind prediction RNN model optimized by each metaheuristic

Method	Learning Rate	Drouput	Epochs	Layers	L1 Neurons	L2 Neurons	L3 Neurons
VMD-RNN-DDHHO	0.010000	0.050755	300	3	97	94	100
VMD-RNN-HHO	0.006340	0.100000	200	1	100	/	/
VMD-RNN-GA	0.009989	0.067669	134	2	95	58	/
VMD-RNN-PSO	0.008124	0.053596	294	3	85	93	73
VMD-RNN-ABC	0.010000	0.100000	300	3	100	79	50
VMD-RNN-FA	0.010000	0.050000	300	2	100	50	/
VMD-RNN-COLSHADE	0.010000	0.096306	300	3	67	50	50
VMD-RNN-SASS	0.010000	0.050000	300	1	64	/	/

Table 10. VMD-RNN-ATT wind energy forecasting objective function overall outcomes

Method	Best	Worst	Mean	Median	Std	Var
VMD-RNN-ATT-DDHHO	0.010359	0.011446	0.010993	0.011361	0.000475	2.254891E-7
VMD-RNN-ATT-HHO	0.010806	0.011496	0.011261	0.011424	0.000269	7.259626E-8
VMD-RNN-ATT-GA	0.011264	0.011672	0.011441	0.011387	0.000152	2.298042E-8
VMD-RNN-ATT-PSO	0.011167	0.011808	0.011455	0.011431	0.000251	6.293247E-8
VMD-RNN-ATT-ABC	0.010911	0.011524	0.011279	0.011259	0.000220	4.861609E-8
VMD-RNN-ATT-FA	0.011160	0.011554	0.011360	0.011420	0.000145	2.108468E-8
VMD-RNN-ATT-COLSHADE	0.011054	0.011368	0.011203	0.011184	0.000126	1.582216E-8
VMD-RNN-ATT-SASS	0.011269	0.011519	0.011392	0.011400	0.000096	9.213128E-9

537 on overall evaluations as well as two and three step ahead. The original HHO performed marginally better
 538 in one step ahead forecasts when considering at the MAE and IA metrics.

539 Further distribution and convergence graphs for the objective function and R^2 are shown in Figure 13
 540 and Figure 14. Accompanying KDE and swarm diversity plots are given in Figure 15.

541 Finally, the selected parameter for the best performing models optimized by each metaheuristic are

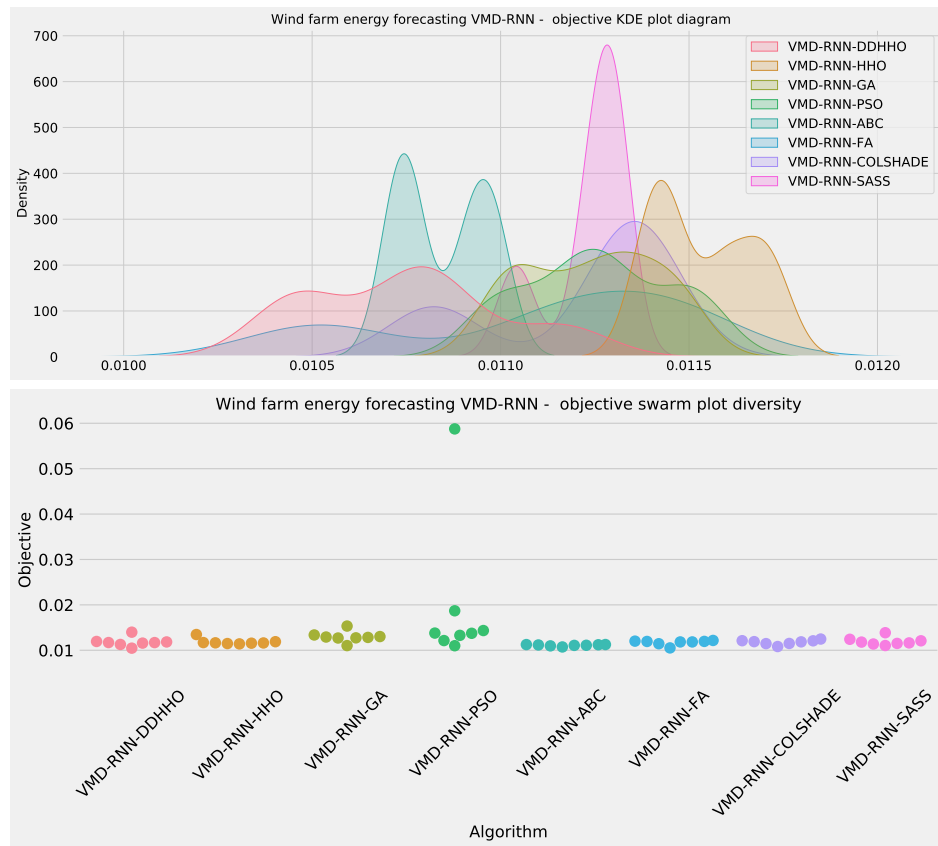


Figure 12. Wind dataset objective swarm and KDE plots for each metaheuristic without attention layer

Table 11. The VMD-RNN-ATT wind energy metrics per each step

Step	Metric	VMD-RNN-ATT-DDHHO	VMD-RNN-ATT-HHO	VMD-RNN-ATT-GA	VMD-RNN-ATT-PSO	VMD-RNN-ATT-ABC	VMD-RNN-ATT-FA	VMD-RNN-ATT-COLSHADE	VMD-RNN-ATT-SASS
One Step	R ²	0.869388	0.868300	0.863840	0.860679	0.861597	0.854800	0.860994	0.853326
	MAE	0.080227	0.079741	0.081451	0.083636	0.081330	0.083773	0.082541	0.083572
	MSE	0.012573	0.012578	0.013107	0.013411	0.013323	0.013977	0.013381	0.014119
	RMSE	0.112129	0.112595	0.114485	0.115806	0.115425	0.118225	0.115676	0.118823
Two Step	IA	0.964787	0.965400	0.963486	0.963898	0.963680	0.961305	0.963349	0.960917
	R ²	0.902255	0.898536	0.892452	0.895950	0.897634	0.898030	0.897528	0.895859
	MAE	0.070517	0.071214	0.073747	0.073326	0.071518	0.071795	0.072607	0.073126
	MSE	0.009409	0.009767	0.010353	0.010016	0.009854	0.009816	0.009864	0.010025
Three Step	RMSE	0.097000	0.098828	0.101748	0.100080	0.099267	0.099074	0.099318	0.100124
	IA	0.973859	0.973364	0.971348	0.972700	0.973169	0.973293	0.973173	0.972177
	R ²	0.912571	0.903750	0.900340	0.902971	0.908152	0.908962	0.908508	0.907307
	MAE	0.067887	0.070822	0.072048	0.071218	0.069180	0.070399	0.072522	0.071352
Overall	MSE	0.008416	0.009265	0.009593	0.009340	0.008841	0.008956	0.009192	0.008923
	RMSE	0.091739	0.096255	0.097946	0.096644	0.094028	0.094636	0.095876	0.094460
	IA	0.976584	0.974331	0.973022	0.973790	0.975383	0.975599	0.974773	0.975041
	R ²	0.894738	0.890195	0.885544	0.886533	0.889128	0.886597	0.887677	0.885497
	MAE	0.0728767	0.073925	0.075749	0.076060	0.074010	0.075322	0.075890	0.076017
	MSE	0.0101326	0.010570	0.011018	0.010922	0.010673	0.010916	0.010812	0.011022
	RMSE	0.1006610	0.102810	0.104965	0.104510	0.103309	0.104481	0.103982	0.104986
	IA	0.9717431	0.971032	0.969285	0.970130	0.970744	0.970066	0.970432	0.969378

542 shown in Table 12.

Table 12. Parameters for best-performing wind prediction RNN-ATT model optimized by each metaheuristic

Method	Learning Rate	Drouput	Epochs	Layers	L1 Neurons	L2 Neurons	L3 Neurons	ATT Neurons
VMD-RNN-DDHHO	0.010000	0.063597	267	3	69	100	50	77
VMD-RNN-HHO	0.010000	0.100000	222	1	74	/	/	54
VMD-RNN-GA	0.007046	0.060227	120	2	66	73	/	74
VMD-RNN-PSO	0.010000	0.050000	234	3	100	50	100	50
VMD-RNN-ABC	0.010000	0.100000	300	3	100	50	50	50
VMD-RNN-FA	0.010000	0.050000	300	3	50	100	81	98
VMD-RNN-COLSHADE	0.005840	0.100000	300	1	91	/	/	86
VMD-RNN-SASS	0.009995	0.100000	255	1	60	/	/	100

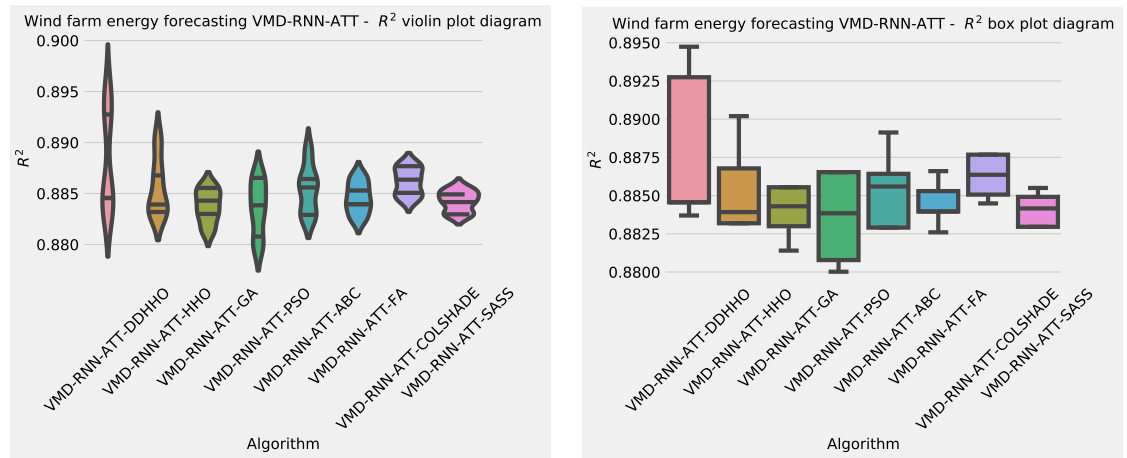


Figure 13. Wind dataset objective function and R^2 distribution plots for each metaheuristic with attention layer

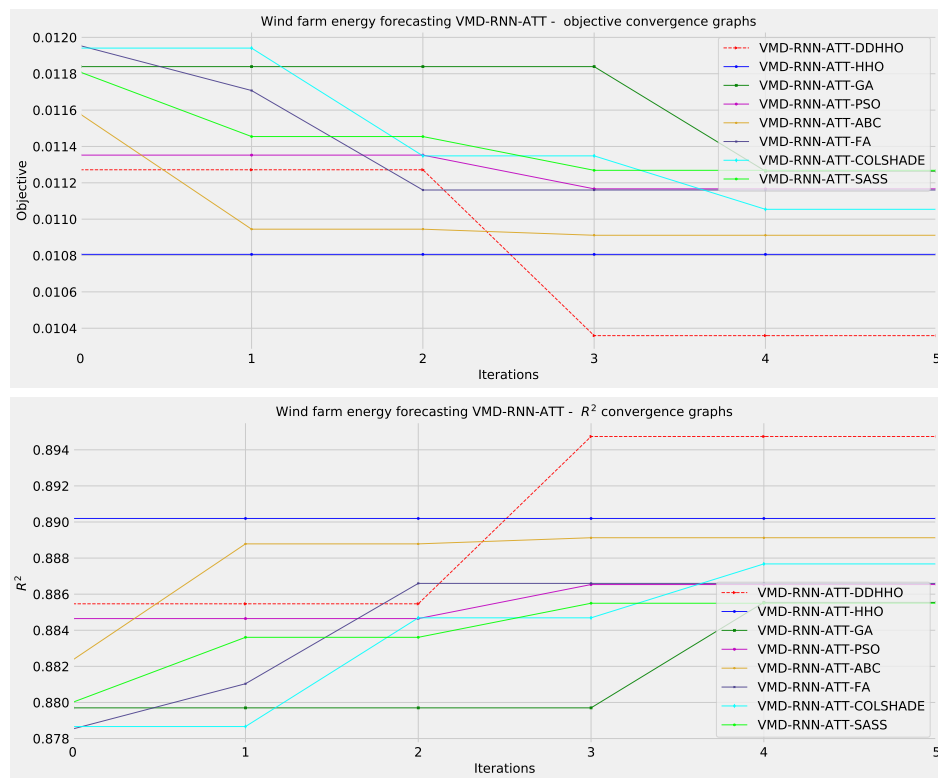


Figure 14. Wind dataset objective function and R^2 convergence plots for each metaheuristic with attention layer

543 6 DISCUSSION, STATISTICAL VALIDATION AND INTERPRETATION.

544 This section presents a discussion of the advantages of the techniques employed in the conducted research,
 545 as well as the statistical analysis of the methods used for comparisons, and the interpretation of the best
 546 models generated for both datasets.

547 6.1 Benefits of using attention mechanism for renewable power generation forecasting

548 The attention mechanism has emerged as a powerful tool in the field of machine learning, particularly
 549 for sequence-to-sequence learning problems like renewable power generation forecasting. By selectively

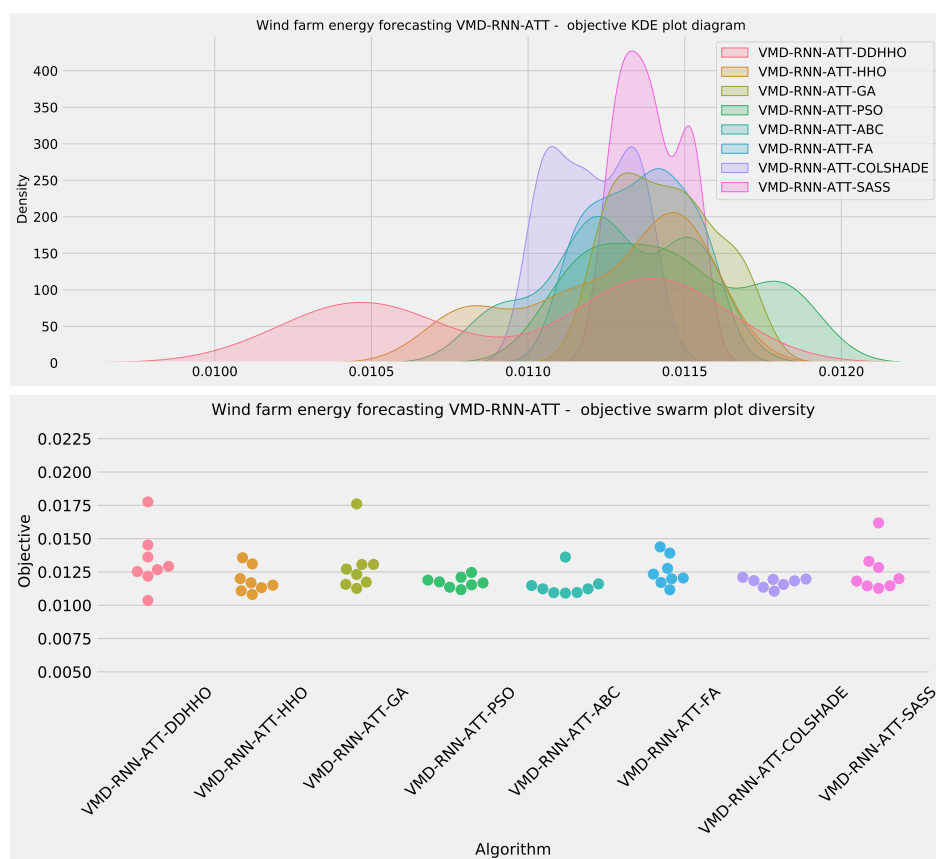


Figure 15. Wind dataset objective swarm and KDE plots for each metaheuristic with attention layer

550 focusing on different parts of the input sequence when generating the output, the attention mechanism can
 551 enhance the performance of forecasting models like the Luong attention-based RNN model. Below, we
 552 discuss the key benefits of using attention mechanisms for renewable power generation forecasting:

553 **1. Improved Long-term Dependency Handling:** Renewable power generation data often exhibit
 554 long-term dependencies due to factors like seasonal patterns and weather trends. Traditional RNN
 555 models can struggle to capture these long-term dependencies effectively, leading to suboptimal forecasts.
 556 Attention mechanisms allow the model to weigh the importance of different parts of the input sequence,
 557 enabling it to focus on the most relevant information for generating the output, thus better handling
 558 long-term dependencies.

559 **2. Enhanced Forecasting Accuracy:** The attention mechanism can lead to more accurate forecasts
 560 by enabling the model to focus on the most relevant parts of the input sequence when generating the
 561 output. This selective focus allows the model to capture the underlying patterns and relationships within
 562 the renewable power generation data more effectively, resulting in improved forecasting performance.

563 **3. Interpretability:** Attention mechanisms provide a level of interpretability to the model's predictions
 564 by highlighting which parts of the input sequence have the most significant impact on the output. This
 565 interpretability can be particularly valuable in renewable power generation forecasting, as it allows domain
 566 experts to gain insights into the factors influencing the model's forecasts and to validate the model's
 567 predictions based on their domain knowledge.

568 **4. Robustness to Noise and Irrelevant Information:** Renewable power generation data can be
 569 subject to noise and irrelevant information (e.g., due to measurement errors or unrelated external factors).
 570 The attention mechanism can help in mitigating the impact of such disturbances on the model's forecasts
 571 by selectively focusing on the most relevant parts of the input sequence and down-weighting the influence
 572 of noise and irrelevant information.

573 **5. Scalability:** Attention mechanisms can scale well with large input sequences, as they allow the
 574 model to focus on the most relevant parts of the input sequence without the need to process the entire

575 sequence in a fixed-size hidden state. This scalability can be particularly beneficial for renewable power
 576 generation forecasting problems, where the input data may consist of long sequences of historical power
 577 generation measurements and environmental variables.

578 **6. Flexibility:** Attention mechanisms can be easily incorporated into various RNN architectures, such
 579 as LSTM and GRU, providing flexibility in designing and adapting the forecasting model for different
 580 renewable power generation scenarios and data characteristics.

581 An additional note needs to be made on attention mechanisms. The attained results suggest that
 582 networks utilizing the attention mechanisms perform slightly worse than the basic RNN. This is likely
 583 due to networks with attention layers having a deeper network architecture and thus require more training
 584 epochs to improve performance.

585 6.2 Benefits of Time Series Decomposition and Integration

586 Incorporating time-series decomposition and integration into the Luong attention-based RNN model can
 587 offer several benefits for renewable power generation forecasting:

588 **1. Improved Forecasting Accuracy:** By decomposing the time-series and accounting for its com-
 589 ponents, the model can better capture the underlying patterns and dependencies in the data, potentially
 590 leading to more accurate and reliable forecasts.

591 **2. Enhanced Model Interpretability:** Decomposition provides insights into the different components
 592 of the time-series, making it easier to understand and interpret the model's predictions in terms of trend,
 593 seasonality, and residual components.

594 **3. Robustness to Noise:** By separating the noise component from the trend and seasonal components,
 595 the decomposition process can help in reducing the impact of noise and outliers on the model's forecasts,
 596 making the model more robust to disturbances.

597 **4. Flexibility and Customizability:** Decomposition and integration techniques can be adapted and
 598 fine-tuned to suit the specific characteristics and requirements of the renewable power generation data,
 599 allowing for a more flexible and customizable forecasting approach.

600 **5. Improved Model Performance:** The integration of decomposed components into the RNN model
 601 can help in better capturing the relationships between the components and the target variable, potentially
 602 leading to improved model performance in terms of generalization and predictive accuracy.

603 6.3 Statistical analysis

604 When considering optimization problems, assessing models is an important topic. Understanding the
 605 statistical significance of the introduced enhancements is crucial. Outcomes alone are not adequate to
 606 state that one algorithm is superior to another one. Previous research suggests Derrac et al. (2011)
 607 that a statistical assessment should take place only after the methods being evaluated are adequately
 608 sampled. This is done by ascertaining objective averages over several independent runs. Additionally,
 609 samples need to originate from a normal distribution so as to avoid misleading conclusions. The use of
 610 objective function averages is still for comparison of stochastic methods is still an open question among
 611 researchers Eftimov et al. (2017). To ascertain statistical significance of the observed outcomes the best
 612 values over 30 independent executions of each metaheuristic have been used for creating the samples.
 613 However, the safe use of parametric tests needed to be confirmed. For this, independence, normality,
 614 and homoscedasticity of the data variances were considered as recommended by LaTorre et al. (2021).
 615 The independence criterion is fulfilled due to the fact that each run is initialized with an pseudo-random
 616 number seed. However, the normality condition is not satisfied as the obtained samples do not stem
 617 from a normal distribution as shown by the KED plots and proved by the Shapiro-Wilk test outcomes for
 618 single-problem analysts Shapiro and Francia (1972). By performing the Shapiro-Wilk test, p -values are
 619 generated for each method-problem combination, and these outcomes are presented in Table 13.

Table 13. Shapiro-Wilk scores for the single-problem analysis for testing normality condition

Experiment	DDHHO	HHO	GA	PSO	ABC	FA	COLSHADE	SASS
Solar VMD-RNN	0.035	0.023	0.022	0.026	0.027	0.030	0.017	0.014
Solar VMD-RNN-ATT	0.035	0.032	0.037	0.019	0.022	0.025	0.037	0.033
Wind VMD-RNN	0.029	0.020	0.025	0.036	0.033	0.019	0.026	0.024
Wind VMD-RNN-ATT	0.021	0.028	0.025	0.037	0.035	0.024	0.026	0.041

620 The standard significance levels of $\alpha = 0.05$ and $\alpha = 0.1$ suggest that the null hypothesis (H_0) can
 621 be refuted, which implies that none of the samples (for any problem-method combinations) are drawn
 622 from a normal distribution. This indicates that the assumption of normality, which is necessary for the
 623 reliable use of parametric tests, was not satisfied, and therefore, it was deemed unnecessary to verify the
 624 homogeneity of variances.

625 As the requirements for the reliable application of parametric tests were not met, non-parametric
 626 tests were employed for the statistical analysis. Specifically, the Wilcoxon signed-rank test, which is
 627 a non-parametric statistical test Taheri and Hesamian (2013), was performed on the DDHHO method
 628 and all other techniques for all three problem instances (experiments). The same data samples used in
 629 the previous normality test (Shapiro-Wilk) were used for each method. The results of this analysis are
 630 presented in Table 14, where p -values greater than the significance level of $\alpha = 0.05$ are highlighted in
 631 bold.

Table 14. Wilcoxon signed-rank test findings

DDHHO vs. others	HHO	GA	PSO	ABC	FA	COLSHADE	SASS
Solar VMD-RNN	0.035	0.046	0.036	0.062	0.043	0.029	0.040
Solar VMD-RNN-ATT	0.041	0.044	0.046	0.035	0.024	0.039	0.037
Wind VMD-RNN	0.024	0.043	0.039	0.052	0.045	0.044	
Wind VMD-RNN-ATT	0.039	0.027	0.025	0.038	0.035	0.042	0.032

632 Table 14, which presents the p -values obtained from the Wilcoxon signed-rank test, demonstrate that,
 633 except for the ABC algorithm in the experiment where VMD-RNN was optimized and validated against
 634 solar and wind datasets, the proposed DDHHO method achieved significantly better performance than
 635 all other techniques in all three experiments. When compared with ABC, the calculated p -value was
 636 slightly above the 0.05 threshold (highlighted in bold in Table 14), suggesting that the DDHHO performed
 637 comparably to ABC. This was expected for the solar dataset, since the ABC in this simulation achieved
 638 moderately better mean value than the DDHHO, as demonstrated in Table 1.

639 The p -values for all other methods were lower than 0.05. Therefore, the DDHHO technique exhibited
 640 both robustness and effectiveness as an optimizer in these computationally intensive simulations. Based
 641 on the statistical analysis, it can be concluded that the DDHHO method outperformed most of the other
 642 metaheuristics investigated in all four experiments.

643 **6.4 Best Model Interpretation and Feature Importance**

644 SHapley Additive exPlanations (SHAP) Lundberg and Lee (2017) is a method that can be utilized to
 645 interpret the outputs of various AI models. Game theory provides a strong basis for SHAP. Though the
 646 use of SHAP the influence real-world factors have on model predictions can be determined. In order to
 647 determine the factors that play the highest role in energy production in solar and wind generation the
 648 best performing models have been subjected to analysis. The outcomes for solar generation are shown in
 649 Figure 16, while wind generation is shown in Figure 17.

650 As demonstrated by Figure 16 a significant influence of previous solar generation instances can be
 651 observed. Cloud cover and humidity play a minor role in forecasting, with cloud cover decreasing the
 652 power produced by the photovoltaic cells.

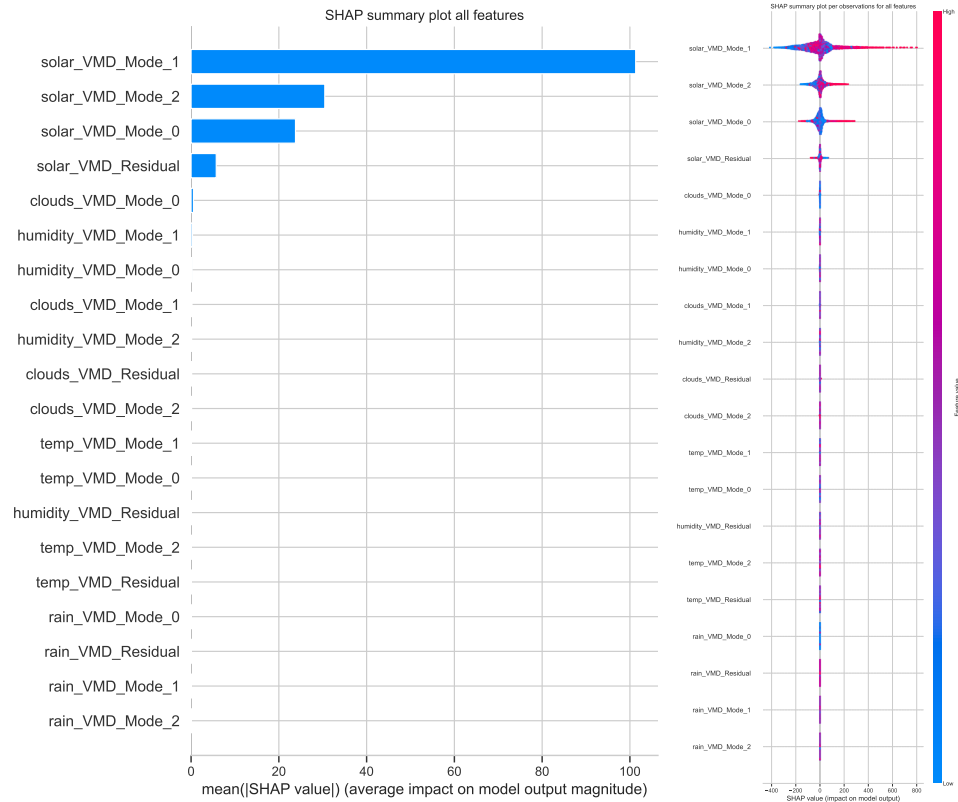


Figure 16. Feature impacts for the best performing RNN model for solar forecasting

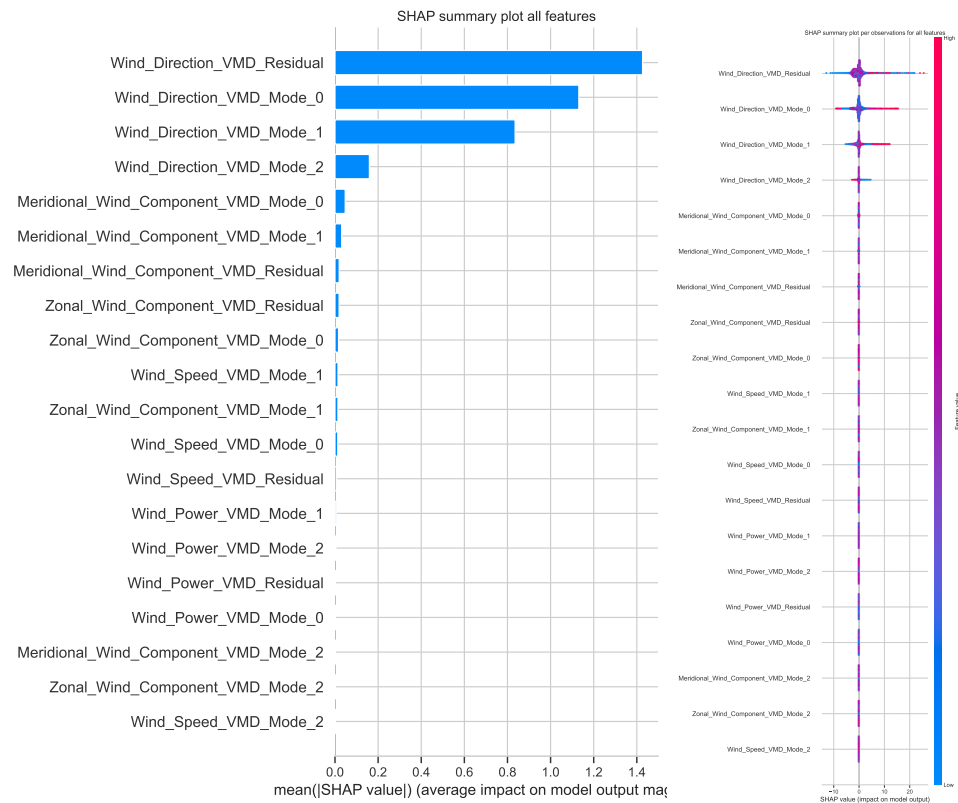


Figure 17. Feature impacts for the best performing RNN model for wind forecasting

653 Indicators from Figure 17 suggest that when forecasting wind power generation wind direction modes
654 have an important role. However, likely due to the sporadic nature of wind bursts wind generation residuals
655 have the highest impact on predictions. Finally, the meridional followed by zonal wind components play a
656 minor role in forecasting.

657 7 CONCLUSIONS

658 This study presents a novel attention-based recurrent neural network model for multistep ahead time-series
659 forecasting of renewable power generation, demonstrating improved forecasting accuracy on both Spain's
660 wind and solar energy datasets and China's wind farm dataset. The Harris Hawk Optimization algorithm
661 is employed for hyperparameter optimization, addressing the challenges posed by the large number of
662 hyperparameters in RNN-type networks. The attention model applied in the second group of experiments
663 provides a weighting system to the RNN, further enhancing the model's performance. The proposed
664 approach has the potential to significantly impact the transition towards a more sustainable future by
665 addressing key challenges related to the storage and management of renewable power generation.

666 As with any work this research has several limitations. Other methods exist for tackling time-series
667 forecasting and their potential remains yet to be explored. Further potential for improvement exist for the
668 HHO, as well as other metaheuristic algorithms yet to be applied to cloud forecasting. Additionally, other
669 approaches for interpreting feature influence exist such as through the analysis of n-Shapley Values.

670 Future research will focus on refining the HHO algorithm for hyperparameter optimization and
671 exploring additional decomposition methods to further improve the forecasting capabilities of the proposed
672 approach, as well as exploring additional metaheuristics applied to cloud load forecasting. Additionally,
673 further methods for feature impact interpretation will be explored.

674 REFERENCES

- 675 Abayomi-Alli, O. O., Sidekerskienė, T., Damaševičius, R., Siška, J., and Połap, D. (2020). *Empirical*
676 *Mode Decomposition Based Data Augmentation for Time Series Prediction Using NARX Network*,
677 volume 12415 LNAI of *Lecture Notes in Computer Science (including subseries Lecture Notes in*
678 *Artificial Intelligence and Lecture Notes in Bioinformatics)*.
- 679 Abuella, M. and Chowdhury, B. (2015). Solar power probabilistic forecasting by using multiple linear
680 regression analysis. In *SoutheastCon 2015*, pages 1–5. IEEE.
- 681 Ali, M. H., Jaber, M. M., Abd, S. K., Rehman, A., Awan, M. J., Vitkutė-Adžgauskienė, D., Damaševičius,
682 R., and Bahaj, S. A. (2022). Harris hawks sparse auto-encoder networks for automatic speech
683 recognition system. *Applied Sciences (Switzerland)*, 12(3).
- 684 Bacanin, N., Jovanovic, L., Zivkovic, M., Kandasamy, V., Antonijevic, M., Deveci, M., and Strumberger,
685 I. (2023a). Multivariate energy forecasting via metaheuristic tuned long-short term memory and gated
686 recurrent unit neural networks. *Information Sciences*, page 119122.
- 687 Bacanin, N., Stoean, C., Zivkovic, M., Rakic, M., Strulak-Wójcikiewicz, R., and Stoean, R. (2023b). On
688 the benefits of using metaheuristics in the hyperparameter tuning of deep learning models for energy
689 load forecasting. *Energies*, 16(3):1434.
- 690 Bas, E., Egrioglu, E., and Kolemen, E. (2021). Training simple recurrent deep artificial neural network
691 for forecasting using particle swarm optimization. *Granul. Comput.* 7, page 411–420.
- 692 Boudraa, A.-O. and Cexus, J.-C. (2007). Emd-based signal filtering. *IEEE transactions on instrumentation*
693 *and measurement*, 56(6):2196–2202.
- 694 Cheng, S. and Shi, Y. (2011). Diversity control in particle swarm optimization. In *2011 IEEE Symposium*
695 *on Swarm Intelligence*, pages 1–9. IEEE.
- 696 Derrac, J., García, S., Molina, D., and Herrera, F. (2011). A practical tutorial on the use of nonparametric
697 statistical tests as a methodology for comparing evolutionary and swarm intelligence algorithms. *Swarm*
698 *and Evolutionary Computation*, 1(1):3–18.
- 699 Dragomiretskiy, K. and Zosso, D. (2013). Variational mode decomposition. *IEEE transactions on signal*
700 *processing*, 62(3):531–544.
- 701 Eftimov, T., Korošec, P., and Seljak, B. K. (2017). A novel approach to statistical comparison of meta-
702 heuristic stochastic optimization algorithms using deep statistics. *Information Sciences*, 417:186–215.
- 703 Foley, A. M., Leahy, P. G., Marvuglia, A., and McKeogh, E. J. (2012). Current methods and advances in
704 forecasting of wind power generation. *Renewable energy*, 37(1):1–8.

- 705 Gurrola-Ramos, J., Hernández-Aguirre, A., and Dalmau-Cedeño, O. (2020). Colshade for real-world
706 single-objective constrained optimization problems. In *2020 IEEE congress on evolutionary computa-*
707 *tion (CEC)*, pages 1–8. IEEE.
- 708 Heidari, A. A., Mirjalili, S., Faris, H., Aljarah, I., Mafarja, M., and Chen, H. (2019). Harris hawks
709 optimization: Algorithm and applications. *Future generation computer systems*, 97:849–872.
- 710 Huang, N. E., Shen, Z., Long, S. R., Wu, M. C., Shih, H. H., Zheng, Q., Yen, N.-C., Tung, C. C., and
711 Liu, H. H. (1998). The empirical mode decomposition and the hilbert spectrum for nonlinear and non-
712 stationary time series analysis. *Proceedings of the Royal Society of London. Series A: Mathematical,*
713 *Physical and Engineering Sciences*, 454(1971):903–995.
- 714 Jouhari, H., Lei, D., Al-qaness, M. A. A., Abd Elaziz, M., Damaševičius, R., Korytkowski, M., and Ewees,
715 A. A. (2020). Modified harris hawks optimizer for solving machine scheduling problems. *Symmetry*,
716 12(9).
- 717 Jovanovic, L., Bacanin, N., Zivkovic, M., Antonijevic, M., Jovanovic, B., Sretenovic, M. B., and
718 Strumberger, I. (2023). Machine learning tuning by diversity oriented firefly metaheuristics for industry
719 4.0. *Expert Systems*, page e13293.
- 720 Jovanovic, L., Jovanovic, D., Bacanin, N., Jovancai Stakic, A., Antonijevic, M., Magd, H., Thiru-
721 malaisamy, R., and Zivkovic, M. (2022). Multi-step crude oil price prediction based on lstm approach
722 tuned by salp swarm algorithm with disputation operator. *Sustainability*, 14(21):14616.
- 723 Karaboga, D. (2010). Artificial bee colony algorithm. *scholarpedia*, 5(3):6915.
- 724 Kennedy, J. and Eberhart, R. (1995). Particle swarm optimization. In *Proceedings of ICNN'95-*
725 *international conference on neural networks*, volume 4, pages 1942–1948. IEEE.
- 726 LaTorre, A., Molina, D., Osaba, E., Poyatos, J., Del Ser, J., and Herrera, F. (2021). A prescription of
727 methodological guidelines for comparing bio-inspired optimization algorithms. *Swarm and Evolution-*
728 *ary Computation*, 67:100973.
- 729 Loe, C. (2022). Energy transition will move slowly over the next decade.
- 730 Lundberg, S. M. and Lee, S.-I. (2017). A unified approach to interpreting model predictions. In Guyon,
731 I., Luxburg, U. V., Bengio, S., Wallach, H., Fergus, R., Vishwanathan, S., and Garnett, R., editors,
732 *Advances in Neural Information Processing Systems 30*, pages 4765–4774. Curran Associates, Inc.
- 733 Medsker, L. and Jain, L. C. (1999). *Recurrent neural networks: design and applications*. CRC press.
- 734 Mirjalili, S. and Mirjalili, S. (2019). Genetic algorithm. *Evolutionary Algorithms and Neural Networks:*
735 *Theory and Applications*, pages 43–55.
- 736 Murariu, M.-G., Dorobanțu, F.-R., and Tärniceriu, D. (2023). A novel automated empirical mode
737 decomposition (emd) based method and spectral feature extraction for epilepsy eeg signals classification.
738 *Electronics*, 12(9):1958.
- 739 Olah, C. and Carter, S. (2016). Attention and augmented recurrent neural networks. *Distill*, 1(9):e1.
- 740 Pascanu, R., Mikolov, T., and Bengio, Y. (2013). On the difficulty of training recurrent neural networks.
741 In Dasgupta, S. and McAllester, D., editors, *Proceedings of the 30th International Conference on*
742 *Machine Learning*, volume 28 of *Proceedings of Machine Learning Research*, pages 1310–1318,
743 Atlanta, Georgia, USA. PMLR.
- 744 Shapiro, S. S. and Francia, R. (1972). An approximate analysis of variance test for normality. *Journal of*
745 *the American statistical Association*, 67(337):215–216.
- 746 Stoean, C., Zivkovic, M., Bozovic, A., Bacanin, N., Strulak-Wójcikiewicz, R., Antonijevic, M., and
747 Stoean, R. (2023). Metaheuristic-based hyperparameter tuning for recurrent deep learning: Application
748 to the prediction of solar energy generation. *Axioms*, 12(3):266.
- 749 Taheri, S. and Hesamian, G. (2013). A generalization of the wilcoxon signed-rank test and its applications.
750 *Statistical Papers*, 54(2):457.
- 751 Tang, Y. and Gibali, A. (2020). New self-adaptive step size algorithms for solving split variational
752 inclusion problems and its applications. *Numerical Algorithms*, 83(1):305–331.
- 753 Wolpert, D. H. and Macready, W. G. (1997). No free lunch theorems for optimization. *IEEE transactions*
754 *on evolutionary computation*, 1(1):67–82.
- 755 Wu, Z. and Huang, N. E. (2009). Ensemble empirical mode decomposition: a noise-assisted data analysis
756 method. *Advances in adaptive data analysis*, 1(01):1–41.
- 757 Yang, X.-S. and He, X. (2013). Firefly algorithm: recent advances and applications. *International journal*
758 *of swarm intelligence*, 1(1):36–50.
- 759 Yang, X.-S. and Slowik, A. (2020). Firefly algorithm. In *Swarm intelligence algorithms*, pages 163–174.

760 CRC Press.

761 Zhang, Y. and Zhao, M. (2023). Cloud-based in-situ battery life prediction and classification using
762 machine learning. *Energy Storage Materials*.

763 Zhao, J., Zhang, B., Guo, X., Qi, L., and Li, Z. (2022). Self-adapting spherical search algorithm with
764 differential evolution for global optimization. *Mathematics*, 10(23):4519.